Reconstruction of Local and Global Marine Redox Conditions During Deposition of Late Ordovician and Early Silurian Organic-Rich Mudrocks in the Siljan Ring District, Central Sweden

by

Xinze Lu

A thesis
presented to the University of Waterloo
in fulfillment of the
thesis requirement for the degree of
Master of Science
in
Earth Sciences

Waterloo, Ontario, Canada, 2015

Authors Declaration

I hereby declare that I am the sole author of this thesis. This is a true copy of the thesis, including any required final revisions, as accepted by my examiners.

I understand that my thesis may be made electronically available to the public.

Abstract

The Ordovician-Silurian transition witnessed the second largest mass extinction in the Phanerozoic Eon and the Hirnantian glaciation. We measured U (as $\delta^{238}U$ relative to standard CRM145 = 0‰) and Mo (as $\delta^{98}Mo$ relative to standard NIST SRM 3134 = +0.25‰) isotope compositions on 26 organic-rich mudrock (ORM) samples of the Late Ordovician (Katian) Fjäcka Shale and the Early Silurian (Rhuddanian-Telychian) Kallholn Formation to infer local and global ocean redox conditions across the Ordovician-Silurian transition. The magnitude of Re, Mo, and U enrichments, Re/Mo and U/Mo ratios, and sedimentary Fe speciation point to euxinic and oxygenated bottom water conditions during deposition of the Fjäcka Shale and upper Kallholn Formation equivalent gray shales, respectively. The same proxies suggest that the more organic-rich samples of the Kallholn Formation were deposited under transiently euxinic conditions with the chemocline situated near the sediment-water interface.

The Mo and U isotope compositions of the most euxinic shales provide the most relevant estimates of the extent of global ocean oxygenation. As expected, the euxinic Fjäcka Shale yields relatively higher average $\delta^{98}Mo$ (0.82‰) of the studied units. Elevated Mo/TOC ratios (average: 13.5 ppm/wt%) of the Fjäcka Shale suggest no more than moderate basin restriction from the open ocean as well as large amounts of Mo in the euxinic bottom waters, which can lead to Mo isotope fractionation between seawater and sediments like that observed in the Cariaco Basin. Hence, we infer that the heaviest Mo isotope composition preserved the euxinic Fjäcka Shale (1.28‰) may be fractionated from contemporaneous seawater. As such, the Mo isotope paleoredox proxy is not reliable on its own. This interpretation is further supported by the high average authigenic

$\delta^{238}U$ (–0.05‰ to 0.02‰; or an average of ~0‰) in the Fjäcka Shale, which is only slightly lower than the modeled value of 0.1‰ for modern euxinic sediments in moderately restricted basins (i.e., between the highly restricted Black Sea [0‰] and open ocean euxinic sediments [0.2‰]). Widespread ocean anoxia should lead to deposition of ORMs with lower $\delta^{238}U$. Hence, the relatively high $\delta^{238}U$ coupled with high Mo, Re, and U enrichments, and high Mo/TOC ratios in the Fjäcka Shale suggest a more oxygenated ocean prior to the Hirnantian glaciation than previously thought, though the extent of oxygenation was less than today. Integration of our data with previous studies further supports the hypothesis that ocean oxygenation intensified from the late Katian to the early-middle Hirnantian in association with global cooling, thus challenging the hypothesis that pronounced ocean anoxia persisted throughout the late Ordovician.

Acknowledgements

I really appreciate my supervisor, Dr. Brian Kendall, for giving me the opportunity to do this amazing project. Without him, I would not have the opportunity to take samples from Colorado State University and do experiments at Arizona State University. Without him, I would not have opportunities to attend annual conference meetings and improve my presentation skills. He was kind and patient answering my questions and concerns. I benefited a lot from him through countless discussions in the office and laboratory.

I would like to thank Dr. Holly J. Stein and Dr. Judith L. Hannah for providing shale samples and their warm welcome when Brian and I arrived at Colorado State University. Their passions and encouragements had a positive impact on me.

I would like to thank Dr. Ariel Anbar for allowing me to do experiments in his world-class clean lab, and Dr. Gwyneth Gordon for her assistance and help regarding U and Mo isotope measurements.

I would like to thank Dr. Chao Li for his measurements on sedimentary Fe speciation. His rapid reply to my questions helped me a lot.

I would like to thank Dr. Jan Ove R. Ebbestad for providing geological background of the Siljan area. It was my pleasure to meet him after my presentation at the *2015 Geological Society of America Annual meeting*. He was very-easy going and we had a nice conversation at the time.

I would like to thank my committee members for their time, advice and support: Dr. Shaun Frape, Dr. Lingling Wu, and Dr. Holly J. Stein. Dr. Shaun Frape was very nice and gave some constructive advice on my conference PPT. I am also grateful to Dr.

Lingling Wu for her efforts and giving me an opportunity to develop the Fe speciation technique with her students. Dr. Tony Endres and Dr. Sherry Schiff supported me when I was a teaching assistant in their courses. Many thanks to Dr. Tony Endres for his care, kindness and support.

I would also like to thank the following colleagues and school mates for their love and support (including but not limited to): Janis Baldwin, Luqi Cui, Jiangyue Ju, Lingyi Kong, Kai Liu, Wanqing Lu, Ning Luo, Fanlong Meng, Alysa Segato, Long Tian, Ryan Truong, Hexin Wang, Jieying Wang, Yinze Wang, and Yan Zhang.

Finally, I would like to thank my parents and parents-in-law for their love and support. My father and father-in-law are excellent role models. Last, but not the least, I want to thank my wife, Xiangnan Liu, for her love and encouragement during my graduate study, and for her amazing strength to be a wonderful wife in a long-distance marriage. I could not finish this without her support.

Table of Contents

List of Figures

List of Tables

1. INTRODUCTION

The unusual climatic conditions of the Ordovician world were quite different than that of the present day and played an important role in biogeographic distributions, metazoan evolution, and extinction. Relatively high sea-level stands (Haq and Schutter, 2008), a giant greenhouse climate state for most of the period (Shields et al., 2003), paleocontinents mostly located in the Southern Hemisphere (Cocks and Torsvik, 2002, 2005), probable superplume events (e.g., Huff et al., 1996; Bergström et al., 2004; Christidis and Huff, 2009), and a terminal Ordovician (Hirnantian) glaciation (e.g., Brenchley et al., 2003; Saltzman and Young, 2005; Delabroye et al., 2010) are the key features of the Ordovician Earth. These unique conditions are associated with rapid biota diversification (the Great Ordovician Biodiversification Event; GOBE) in the early-middle Ordovician (e.g., Webby et al., 2004) and the second largest Phanerozoic extinction event in the late Ordovician, with approximately 86% loss of species (Brenchley et al., 2001; Sheehan, 2001). The surviving species and communities reconstructed the ecology to pre-extinction levels (similar to the early Ordovician) for at least 4-5 Ma in the Silurian (Brenchley et al., 2001; Sheehan, 2001). In addition to studying the early to middle Ordovician Period associated with the GOBE, understanding the rapidly changing environment during the late Ordovician to early Silurian is also important to constrain the relationships between biology, ocean redox conditions, and climate change.

The early-middle part of the late Ordovician (Sandbian and Katian) was characterized by high sea levels in the Paleozoic, which were generally over 150 meters

higher than that of the present day (Haq and Schutter, 2008; Fig. 1). Sea surface temperature (SST) variations based on clumped oxygen isotope data from carbonates and oxygen isotope data from conodont apatite show a general cooling trend during this time (Trotter et al., 2008; Finnegan et al., 2011; Fig. 1). A short warming interval named the "Boda Event" occurred in the late Katian, based on migrations of benthic species from low to high latitude and the occurrence of warm water near the South Pole (Fortey and Cocks, 2005), which is also suggested by SST variation profiles (Fig. 1; Finnegan et al., 2011; Melchin et al., 2013). However, other authors consider the "Boda Event" to mark global cooling, as evidenced by the widespread Chatfieldian carbon isotope ($\delta^{13}C_{carb}$) excursion (Saltzman and Young, 2005) and detailed facies analysis (Cherns and Wheeley, 2007).

Regardless, a mass extinction event occurred in the following Hirnantian Stage, which consists of two phases. Rapid cooling is thought to be the main kill mechanism for the first extinction phase during the early to middle Hirnantian (Brenchley et al., 2001; Melchin et al., 2013). The Hirnantian glaciation ended the giant greenhouse environment of the preceding Ordovician, and resulted in rapid cooling and eustatic sea level fall (Fig. 1; Finnegan et al., 2011). This major glaciation is also characterized by a strong positive $\delta^{13}C_{carb}$ excursion (HICE: Hirnantian Isotope Carbon Excursion) (Fig. 1; e.g., Marshall and Middleton, 1990; Brenchley et al., 1994; Kump et al., 1999; Webby et al., 2004; Bergström et al., 2006; LaPorte et al., 2009; Ainsaar et al., 2010), which can be explained by either increased burial of organic carbon triggered by increased thermohaline circulation of the ocean (Brenchley et al., 1994), or the weathering of carbonate platforms (with high $\delta^{13}C$) in low latitudes due to an eustatic sea level fall (Kump et al., 1999).

Evidence for increasing oxygenation at this time is mainly based on a switch from deposition of black shales to gray shales (e.g., Finney et al., 1999; LaPorte et al., 2009). The second phase of the mass extinction occurred during the middle Hirnantian, which is thought to be associated with a return of widespread ocean anoxia following the demise of the glaciation (Brenchley et al., 2001; Melchin et al., 2013). A long-term rise in sea level occurred during the early Silurian due to the protracted melting of glaciers (Fig. 1) (e.g., Melchin et al., 2013).

Figure 1

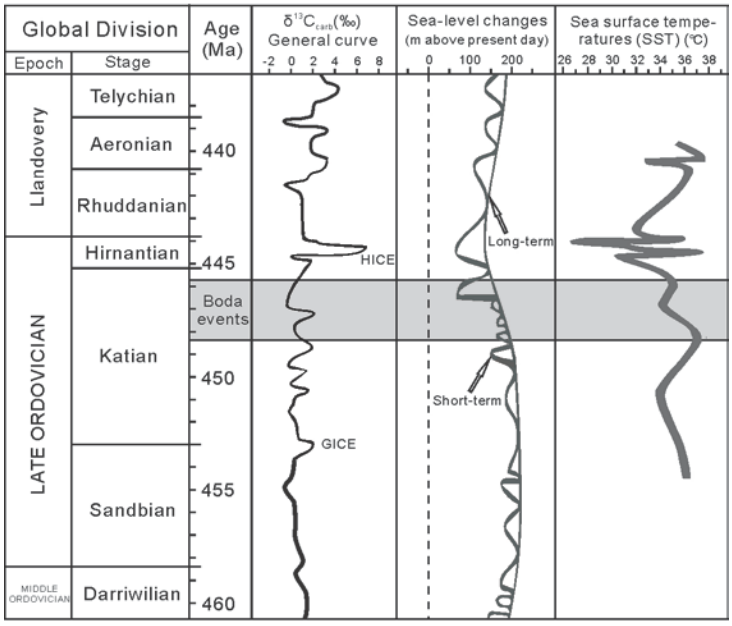

Fig. 1. Carbonate carbon isotope, eustatic sea level, and sea surface temperature variations during the middle-late Ordovician to early Silurian. Global division of the geologic time scale is from Cohen et al. (2013). Carbonate carbon isotope curve is modified from Bergström et al. (2009) and Cramer et al. (2011). Eustatic sea level curve is sourced from Haq and Schutter (2008). Sea surface temperature curve is from Finnegan et al. (2011).

Besides the application of traditional light stable isotopes and radiogenic isotopes (e.g., $\delta^{13}C$, $\delta^{18}O$, $^{87}Sr/^{86}Sr$) to infer environmental changes in the past, non-traditional metal isotope systems like Mo have recently been used to infer global ocean redox conditions (e.g., Barling et al., 2001; Siebert et al., 2003, 2006; Arnold et al., 2004; Nägler et al., 2005, 2011, 2014; Neubert et al., 2008; Gordon et al., 2009; Dahl et al., 2010a, 2010b, 2011; Duan et al., 2010; Herrmann et al., 2012; Kendall et al., 2009, 2011, 2015; Noordmann et al., 2015). The Mo isotope composition of euxinic organic-rich mudrocks (ORMs) may directly capture the global seawater Mo isotope composition (Barling et al., 2001; Arnold et al., 2004; Neubert et al., 2008). Molybdenum isotope compilations through time reveal that the $\delta^{98}Mo$ of global seawater between 520 and 440 Ma reaches up to 1.5‰, with one exception (2.4‰) in the early Hirnantian associated with glaciation (Dahl et al., 2010b; Zhou et al., 2012, 2015; Kendall et al., 2015). However, Zhou et al. (2012, 2015) do not interpret this high $\delta^{98}Mo$ value as evidence for widespread ocean oxygenation, but instead as a local intensification of ocean anoxia in the Yangtze Sea (South China). The otherwise uniformly low seawater $\delta^{98}Mo$ values during 520−440 Ma are similar to that of Middle Proterozoic seawater (Dahl et al., 2010b; Kendall et al., 2009, 2011) but significantly lower than modern seawater (2.34 ± 0.10‰; Barling et al., 2001; Siebert et al., 2003; Nakagawa et al., 2012; Nägler et al., 2014). This observation suggests a generally less oxygenated environment from the middle Cambrian to the early Silurian compared with today.

However, significant fluctuations in ocean redox conditions across the Ordovician-Silurian transition may have occurred, as has been hypothesized for the Ediacaran-Cambrian interval (Dahl et al., 2010b; Sahoo et al., 2012; Kendall et al., 2015).

For instance, the Hirnantian glaciation may have been associated with increased ocean circulation and oxygenation (Brenchley, 1989; Melchin et al., 2013). In contrast, expansions of ocean anoxia were proposed as the kill mechanism for both the early-middle and middle-late Hirnantian extinctions (Hammarlund et al., 2012). This controversy indicates that the relative magnitudes of oxic and anoxic conditions are not well known. Molybdenum isotope data and other indicators of global ocean redox conditions are not abundant for the Ordovician-Silurian transition. Only three studies report Mo isotope data from ORMs deposited during this time interval (Dahl et al., 2010b, Zhou et al., 2012, 2015). Some of the Mo isotope data may not reflect the global seawater composition because of Mo isotope fractionation between the seawater and sediments due to non-euxinic conditions or incomplete removal of Mo from local bottom waters (Dahl et al., 2010b; Kendall et al., 2015). Hence, more data and new global redox proxies are needed to better understand global ocean redox conditions at this time. In this regard, the U isotope system in ORMs represents an emerging global ocean paleoredox proxy with good potential (Weyer et al., 2008; Montoya-Pino et al., 2010; Kendall et al., 2013, 2015).

In this study, the research objective is to use a combination of sedimentary Fe speciation, trace metal concentrations, and Mo and U isotope data on ORMs deposited before and after the Hirnantian to better constrain local and global marine redox conditions. The combined use of the Mo and U isotope systems represents a more robust approach towards inferring global ocean redox conditions compared with using the Mo isotope system alone (Kendall et al., 2015).

2. GEOLOGICAL BACKGROUND

The Siljan ring district (61.04°N, 14.92°E) is located in central Sweden with a present-day diameter of 52 km (Grieve, 1988), and is thought to be the largest impact structure in Europe (Fig. 2). Holm et al. (2011) estimated a crater diameter of 90 km before erosion. The earliest research on the Siljan impact structure can be traced back to the 18th century and is summarized in Ebbestad and Högström (2007). Recently, the Siljan ring has become a focus of research as part of the project "Concentric Impact Structures in the Paleozoic" (CISP; Högström et al., 2010), which is also one of the essential parts of the "Swedish Deep Drilling Program" (SDDP; Lorenz et al., 2010) (Fig. 2). Since 2011, three drillholes (Mora 001, Solberga #1, and Stumsnäs #1) in the Siljan area were drilled by the Swedish private company IGRENE AB for geothermal energy and natural gas exploration.

Figure 2

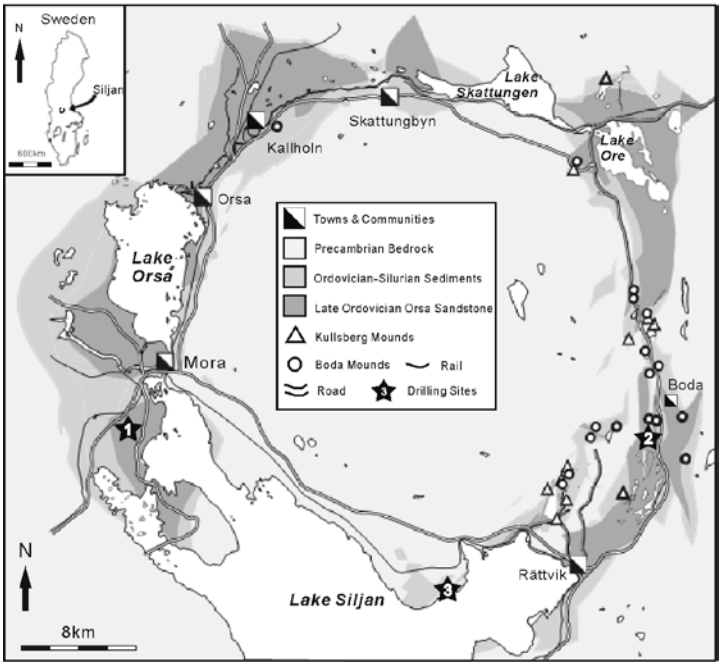

Fig. 2. Simplified map of the Siljan ring district showing new drill sites (1, Mora 001; 2, Solberga #1; 3, Stumsnäs #1). Modified from Ebbestad and Högström (2007).

The ancient continent Baltica moved north during the early Paleozoic and was situated at low latitudes near the equator during the late Ordovician (Cocks and Torsvik, 2002, 2005). At that time, the depositional environment represented by the Siljan area was located on the shallow continental shelf (Cocks and Torsvik, 2005). The sub-Cambrian peneplain formed during the late Precambrian under stable geological conditions and denudation, and is widely recognized in southern Sweden (e.g., Cederbom et al., 2000; Huigen and Andriessen, 2004). Subsequently, early Paleozoic sediments covered its surface, and stratigraphic studies of these rocks revealed a basin deepening to the west (Larson et al., 1999; Cederbom et al., 2000). The Scandinavian Caledonides developed from the late Silurian to the early Devonian due to collision between Baltica and Laurentia (e.g., Cederbom et al., 2000; Huigen and Andriessen, 2004). Sedimentary records in the Oslo area indicate the infill and development of Caledonian foreland basin (Huigen and Andriessen, 2004). Due to rapid uplift and erosion of Baltica, eroded rocks were transported towards further east during the middle Devonian and Carboniferous (Huigen and Andriessen, 2004). The modern Swedish landscape was shaped after final exhumation of the rocks in the Mesozoic and Tertiary.

The Siljan structure is thought to have been caused by the impact of a meteorite on sedimentary rocks of Ordovician and Silurian age. Evidence for a bolide impact origin includes planar deformation structures in quartz (Tamminen and Wickman, 1980), occurrence of shatter cones (Svensson, 1973), and fluid inclusion analyses (Komor et al., 1988). New $^{40}Ar/^{39}Ar$ laser spot data and step-heating data for a melt breccia indicate an

impact event age of 380.9 ± 4.6 Ma (Reimold et al., 2005; Jourdan et al., 2012). Precambrian bedrock is mainly exposed in this ring-like depression, particularly in the central plateau that is about 30 km wide (Fig. 2). However, a few localities expose Ordovician and Silurian strata around the impact margins, thus providing opportunities to study the regional early Paleozoic sedimentary sequence and paleoenvironments (Ebbestad and Högström, 2007; Lehnert et al., 2012, 2013). Outcrops are highly metamorphosed and deformed by the impact event; however, the early Paleozoic sedimentary rocks underneath are well preserved.

The Tremadocian Obolus beds of basal Ordovician age represent the beginning of the preserved Paleozoic lithostratigraphic succession, which ends with the youngest Nederberga Formation shales of middle Silurian age (Grahn, 1998; Ebbestad and Högström, 2007). The Ordovician stratigraphy is well preserved and similar to that observed in other parts of Sweden (e.g., Ebbestad and Högström, 2007; Lehnert et al., 2012). The regional geological succession and lithostratigraphy are summarized by Ebbestad and Högström (2007). More recently, a geological correlation of the terminal Ordovician succession based on carbon isotope stratigraphy and biostratigraphy from five quarries and eight sections was presented by Ebbestad et al. (2014) (Fig. 3). The ages for the stratigraphic layers in the Siljan ring district are indicated by well-characterized biozones (Ebbestad and Högström, 2007; Ebbestad et al., 2014).

Figure 3

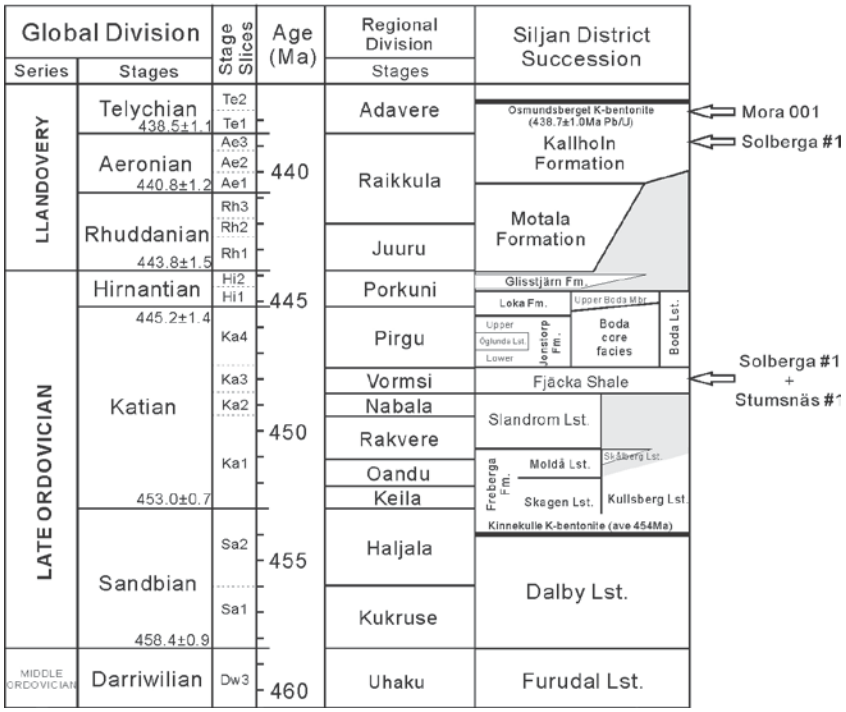

Fig. 3. Siljan ring district stratigraphy from the late Ordovician to early Silurian. Global division of the geologic time scale is from Cohen et al. (2013). Stage slices are based on Bergström et al. (2009) and Cramer et al. (2011). Regional stages are from Nõlvak et al. (2006) and Ebbestad et al. (2014). Stratigraphic succession of the Siljan ring district is based on Ebbestad and Högström (2007) and Ebbestad et al. (2014). The ages of the Osmundsberget K-bentonite and Kinnekulle K-bentonite are from Bergström et al. (2008) and Bauert et al. (2014), respectively. Drill core names and arrows on the right side indicate the stratigraphic layers sampled and their ages.

It was once proposed that petroleum at the impact site is of mantle origin based on the deep Earth gas hypothesis (Gold and Soter, 1980). However, subsequent drilling tests and geophysical research were not consistent with a mantle origin (Juhlin, 1990; Papasikas and Juhlin, 1997). Geochemical data further point to an organic origin for the petroleum. Oil-source rock correlation analysis based on biomarkers and carbon isotope data indicate that the Siljan oil was sourced predominantly from the Ordovician Fjäcka Shale ("Tretaspis shale"), probably with a minor contribution from shales of the Silurian

Kallholn Formation ("Rastrites shale") (Vlierboom et al., 1986; Ahmed et al., 2014). The burial depth (≤ 2 km) of these source rocks is shallow and thus the temperature was not high enough to produce mature ORMs with respect to hydrocarbon potential via the normal process of deep source rock burial (Stein et al., 2014). Hence, oil produced from these ORMs is likely a result of rapid heating during and immediately following the bolide impact (Larson et al., 1999; Stein et al., 2014).

Specifically, the outcrops of Kullberg and Boda limestone mostly appear at the southeastern part of the Siljan ring district, providing valuable opportunities for sampling oil seeps (Stein et al., 2014). Stein et al. (2009, 2014) reported a 4-point Re-Os date of 812 ± 48 Ma for oil seeps recovered from the Boda limestone in the Solberga quarry. The four oil samples have constant Re (1.4-1.6 ppb) but highly variable Os concentrations (40-300 ppt) that are interpreted as mixtures of meteoritic debris and oil (Stein et al., 2014). Thus, the generated 4-point Re-Os regression represents a mixing line between meteoritic material and shale-derived oil rather than an isochron (Stein et al., 2014). Compared with the late Ordovician seawater $^{187}Os/^{188}Os$ ratio of 0.4-1.0 (e.g., Finlay et al., 2010), the initial $^{187}Os/^{188}Os$ (0.20 ± 0.12) from the Re-Os regression indicates an unradiogenic extraterrestrial source. Although the Re-Os system in oil was significantly disturbed by inclusion of meteoritic material during hydrocarbon formation, there is no disturbance to the shales (Stein et al., 2009, 2014).

For this study, all the samples (n=26) come from the Mora 001, Solberga #1, and Stumsnäs #1 drill cores. The lithostratigraphic units and detailed core descriptions are reported in Lehnert et al. (2012, 2013). The absence of late Ordovician stratigraphic layers in Mora 001 from the western part of the Siljan ring has been explained as tectonic

loading during the movement of the Caledonian peripheral forebulge. Hence, the upper Ordovician rock units are missing in the western part of the Siljan ring whereas these rock units are preserved in the eastern part (Lehnert et al., 2012).

Six samples of early Silurian light gray shale were obtained from a “lower shale member” that has a thickness of about 62 m in Mora 001. Based on new graptolite findings, the gray shale (early Telychian) is broadly equivalent to the upper Kallholn Formation (Aeronian-Telychian) (Lehnert et al., 2013). In Solberga #1, located in the eastern Siljan ring, the thickness of the Kallholn Formation and Fjäcka Shale is 60 m and 12 m, respectively. Four samples of the Kallholn Formation and six samples of the Fjäcka Shale were obtained from Solberga #1. Stumsnäs #1 was drilled in the southern Siljan ring. The Fjäcka Shale has a thickness of 5 m at this locality and 10 samples were obtained from this drill core.

3. ANALYTICAL METHODS

3.1. Sample dissolution and element concentrations

Trace element concentrations and U and Mo isotope compositions were measured in a clean laboratory at the W.M. Keck Foundation Laboratory for Environmental Biogeochemistry, School of Earth and Space Exploration, Arizona State University. Samples were powdered in a ball mill using silicon nitride jars. In our initial experiments, about 1 g of each powdered sample was ashed at 550°C overnight to remove organic matter. Several rounds of concentrated HF–HNO_3–HCl acid digestions were performed in 22 mL Savillex Teflon beakers. However, the samples did not completely dissolve.

Decreased sample volumes and hot plate stains following dissolution indicated that partial loss of many sample solutions from the closed Teflon beakers occurred because of high volatile pressure. Sample loss was confirmed by erroneous, consistently low element concentrations (by 50-60%) for a 1 g digest of the USGS Devonian black shale standard SDO-1. Hence, dissolution of gram-sized quantities of shale powders in 22 mL Savillex Teflon beakers is not recommended. To obtain accurate elemental data, 0.1 g of each powdered sample was re-ashed and re-digested in HF–HNO_3–HCl. This time, each sample was completely dissolved without any loss (confirmed by accurate SDO-1 element concentrations).

A weighed split of each sample solution was diluted with 0.32M HNO_3 and major and trace element concentrations were analyzed using a Thermo i-CAP quadrupole inductively coupled plasma mass spectrometer (Q-ICP-MS). The element concentrations of a 0.1 g digest of SDO-1 was used to verify instrument accuracy. Trace element concentration reproducibility was within 10%.

To further evaluate local redox conditions, enrichment factors (EFs) of U, Mo, and Re were calculated relative to average upper crust. The EF is calculated as follows (Tribovillard et al., 2006):

$$EF = [metal / Al]_{sample} / [metal / Al]_{average\ upper\ crust}$$

The average upper crust data for U (2.8 ppm), Mo (1.5 ppm), and Al (8.04%) are from McLennan (2001). The average upper crustal Re concentration is assumed to be 1.0 ppb based on Selby et al. (2007).

3.2. Uranium isotope analysis

Uranium isotope measurements followed the experimental procedures stated in Weyer et al. (2008) and Kendall et al. (2013). A weighed amount of double spike solution (^{233}U and ^{236}U) was added to a split of each digested sample solution to correct for column chromatography and instrument mass bias. Eichrom® UTEVA resin was used to isolate and purify U from sample solutions. Uranium isotope measurements were performed on a Thermo Scientific Neptune multiple collector (MC) ICP-MS instrument using an ESI Apex desolvating nebulizer. The U isotope ratio ($\delta^{238}U$) of each sample was reported relative to the CRM145 standard:

$$\delta^{238}U_{\text{sample}}\ (‰) = (^{238/235}U_{\text{sample}} / {}^{238/235}U_{\text{CRM145}} - 1) \times 1000$$

Repeated measurements of the U isotope standards CRM145 (measured against itself) and CRM129a yielded average $\delta^{238}U$ of 0.00 ± 0.09‰ (2SD, n=87) and –1.70 ± 0.10‰ (2SD, n=8), respectively. The average value for CRM129a is statistically identical to that reported by earlier studies (Brennecka et al., 2011a; Kendall et al., 2013, 2015). During the course of this study, the SDO-1 standard was also analyzed and yielded an average $\delta^{238}U$ of –0.11 ± 0.10‰ (2SD, n=3), which is in agreement with the average of –0.06 ± 0.04 ‰ (2SD, n=17) reported for SDO-1 by Kendall et al. (2015). The 2SD uncertainty of a sample is reported as the 2SD uncertainty of sample replicate measurements or 0.09‰ (the average uncertainty of CRM145, CRM129a, and SDO-1), whichever is greater.

3.3. Molybdenum isotope analysis

The measurements of Mo isotope compositions followed the protocols stated in Duan et al. (2010), Kendall et al. (2011), and Herrmann et al. (2012). A weighed amount of double spike (^{97}Mo and ^{100}Mo) was added to a split of each digested sample solution to correct for instrumental and column chromatography mass fractionation. Subsequently, the purification of Mo was carried out by a two-step column chemistry procedure that involves first anion and then cation exchange chromatography (Barling et al., 2001; Arnold et al., 2004; Duan et al., 2010). Molybdenum isotope analysis was performed on the Neptune MC-ICP-MS instrument using an ESI Apex desolvating nebulizer (e.g., Dahl et al., 2010b).

Molybdenum isotope data for samples are first measured relative to an in-house standard (RochMo2) and then are re-calculated relative to the new international NIST SRM 3134 standard (Nägler et al., 2014). Thus, Mo isotope data are reported as follows (Nägler et al., 2014):

$$\delta^{98}\text{Mo}_{\text{sample}}\,(‰) = [(^{98/95}\text{Mo}_{\text{sample}} / {}^{98/95}\text{Mo}_{\text{NIST SRM 3134}} \times 0.99975) - 1] \times 1000$$

After setting the δ^{98}Mo of NIST SRM 3134 to 0.25‰, the δ^{98}Mo of open ocean seawater is 2.34 ± 0.10‰ (2SD) (Goldberg et al., 2013; Nägler et al., 2014), which is statistically identical (given analytical uncertainties) to the seawater value (~2.3‰) previously measured against in-house standards in different labs (Barling et al., 2001; Siebert et al., 2003; Arnold et al., 2004; Nakagawa et al., 2012). In this way, the "traditional" seawater δ^{98}Mo value of ~2.3‰ can be kept and Mo isotope data measured relative to in-house

standards in most labs can now be directly compared after re-normalizing to NIST SRM 3134 (Goldberg et al., 2013; Nägler et al., 2014).

The NIST SRM 3134 standard has a heavier Mo isotope composition (0.33 ± 0.05‰; 2SD, n = 99) compared with the in-house RochMo2 standard at ASU (Goldberg et al., 2013). In this study, the measured value for NIST SRM 3134 was 0.31 ± 0.04‰; 2SD, n = 10) relative to RochMo2. Hence, 0.06 ‰ was subtracted from each sample Mo isotope composition measured relative to RochMo2 so that all data is reported relative to NIST SRM 3134 = 0.25 ‰. The average δ^{98}Mo for SDO-1 in this study was 1.06 ± 0.05‰ and 0.81 ± 0.05‰ (2SD, n = 13) normalized to NIST SRM 3134 = 0.25‰ and 0.00‰, respectively. The latter value is in excellent agreement with the average δ^{98}Mo values for SDO-1 of 0.80 ± 0.14‰ (2SD, n = 145) reported by Goldberg et al. (2013) for multiple laboratories, and 0.82 ± 0.11 ‰ (2SD, n = 145) reported by Goldberg et al. (2013) for double spike analyses using the ASU Neptune MC-ICP-MS. Given the average uncertainty of SDO-1, we report the 2SD uncertainty of a sample as the 2SD uncertainty of sample replicate measurements or 0.11 ‰, whichever is greater.

3.4. Sedimentary iron speciation

The Mo isotope composition in euxinic sediments is more likely to reflect the coeval seawater Mo isotopic composition than non-euxinic sediments (Barling et al., 2001; Arnold et al., 2004; Gordon et al., 2009). Sedimentary Fe speciation is a useful independent proxy that has been widely used to evaluate local bottom water redox conditions for paleoenvironmental studies (e.g., Poulton and Raiswell, 2002; Anderson and Raiswell, 2004; Poulton et al., 2004, 2010; Lyons and Severmann, 2006; Canfield et

al., 2007; Reinhard et al., 2009; Kendall et al., 2010, 2011, 2015; Poulton and Canfield, 2011). Biogeochemically highly reactive iron (Fe_{HR}), which can react with sulfide in the water column or in sediments, is mainly composed of pyrite Fe (Fe_{py}) and other Fe phases, including carbonate Fe (Fe_{carb}), ferric oxide Fe (Fe_{ox}), and magnetite Fe (Fe_{mag}). Thus, highly reactive Fe is defined as follows (Poulton et al., 2004; Poulton and Canfield, 2005): $Fe_{HR} = Fe_{carb} + Fe_{ox} + Fe_{mag} + Fe_{py}$. Total Fe ($Fe_T$) consists of unreactive or poorly reactive Fe complexed with silicate minerals and the aforementioned highly reactive Fe species (Poulton et al., 2004).

It was found that the ratios of highly reactive Fe to total Fe (Fe_{HR}/Fe_T) in modern sediments (average = 0.26 ± 0.08; Raiswell and Canfield, 1998) and Phanerozoic sedimentary rocks (average = 0.14 ± 0.08; Poulton and Raiswell, 2002) have an upper limit of 0.38 for oxygenated marine settings. Sediments and sedimentary rocks that have higher ratios beyond this threshold were deposited from anoxic waters. However, analyses on Phanerozoic sediments and sedimentary rocks suggest that 0.22 is a reasonable lower limit to distinguish oxic from anoxic conditions in local bottom waters (Poulton and Raiswell, 2002; Poulton and Canfield, 2011). Hence, Fe_{HR}/Fe_T can be used to distinguish anoxic conditions (≥ 0.38) from oxic conditions (≤ 0.22). Samples with ratios between 0.22 and 0.38 may be oxic or anoxic, depending on local factors such as sedimentation rates or depletion of Fe_{HR} during diagenesis and metamorphism (Poulton and Canfield, 2011). Independent evidence is thus needed to distinguish between oxic and anoxic conditions when Fe_{HR}/Fe_T is between 0.22 and 0.38 (e.g., Re/Mo and U/Mo ratios). High Fe_{HR}/Fe_T ratios in fine-grained sediments are either caused by formation of pyrite in euxinic waters, or by formation of other Fe phases (carbonate, magnetite, or

ferric oxides) whose Fe(II) was derived from anoxic (sulfide-free) waters (Anderson and Raiswell, 2004).

In anoxic environments ($Fe_{HR}/Fe_T \geq 0.22$-0.38), ferruginous and euxinic conditions can be distinguished by using the extent of pyritization of the highly reactive iron pool (Fe_{py}/Fe_{HR}). Anderson and Raiswell (2004) proposed that $Fe_{py}/Fe_{HR} = 0.8$ is a lower limit for euxinia when studying Black Sea sediments. Subsequently, this value was redefined because it should be lower using a new extraction scheme for iron and taking highly reactive Fe_{carb} and Fe_{mag} into account (Poulton and Canfield, 2005, 2011). Hence, $Fe_{py}/Fe_{HR} = 0.7$ is a more appropriate boundary value to distinguish ferruginous from euxinic conditions based on analyses of Phanerozoic sediments and sedimentary rocks (März et al., 2008; Poulton and Canfield, 2011).

Sedimentary Fe speciation analyses were performed at the State Key Laboratory of Biogeology and Environmental Geology, China University of Geoscience, Wuhan, China. A sequential extraction method (Poulton and Canfield, 2005) was used, and the Fe contents of the carbonate (Fe_{carb}), ferric oxide (Fe_{ox}), and magnetite (Fe_{mag}) fractions were determined by Q-ICP-MS (Li et al., 2010). Disseminated pyrite was extracted and measured using the chromium reduction method (Canfield et al., 1986), and the Fe content in pyrite (Fe_{py}) was then calculated based on a pyrite mineral formula of FeS_2 (Li et al., 2010).

3.5. Total organic carbon

Total organic carbon (TOC) contents were analyzed by Activation Laboratories Ltd. The TOC is determined as the difference between total carbon (TC) and total

inorganic carbon (TIC). The TC was analyzed on an ELTRA CS 2000 Carbon Sulphur Analyzer. A split of the sample powder was weighed, mixed with iron chips and a tungsten accelerator, and then combusted at 1370°C in a nearly pure oxygen environment. After removal of moisture and dust, the amount of CO_2 and SO_2 produced during combustion was determined by a solid-state infrared detector. Subsequently, CO_2 gas was dissolved with 2N perchloric acid and titrated by a UIC coulometer to obtain the amount of TC. A separate split of sample powder was ignited at 600°C to remove only organic carbon, enabling the amount of TIC to be quantified using the same measurement procedure as described above. This procedure results in a detection limit of 0.5 wt% for TOC content.

4. RESULTS

4.1. Total organic carbon, sedimentary iron speciation, and trace metal concentrations

The Fjäcka Shale contains high TOC (4.0−8.2%) contents with an average of 5.56% (Table 1 and Fig. 4). High ratios of Fe_{HR}/Fe_T (> 0.38) and Fe_{py}/Fe_{HR} (> 0.79) clearly indicate a euxinic depositional environment for the Fjäcka Shale at both the Stumsnäs #1 and Solberga #1 localities (Fig. 4 and Fig. 5a). This observation is consistent with high U (12.4−17.1 ppm), Mo (14.1−226.9 ppm), and Re (21.9−79.2 ppb) concentrations (Table 1 and Fig. 4), and high Mo/U and Mo/Re ratios (Fig. 5).

Table 1. Geochemical data for shales from the Mora 001, Solberga #1, and Stumsnäs #1 drillholes in the Siljan ring district, central Sweden

Sample	TOC[a] (%)	Al (wt%)	U (ppm)	Mo (ppm)	Re (ppb)	Mo/TOC (ppm/%)	U EF[b]	Mo EF[b]	Re EF[b]	$\delta^{238}U$[c] (‰)	2SD Measured	2SD[d] Reported	n[e]	$\delta^{98}Mo$[f] (‰)	2SD Measured	2SD[g] Reported	n[e]	Fe_{Carb} (wt%)	Fe_{Ox} (wt%)	Fe_{Mag} (wt%)	Fe_{PY} (wt%)	Fe_{HR}[h] (wt%)	Fe_T[I] (wt%)	Fe_{HR}/Fe_T	Fe_{PY}/Fe_{HR}
Mora 001 - Gray shales (upper Kallholn Fm. Equivalent)																									
181.64	<0.5	7.0	5.3	7.4	8.9	N/A	2.2	5.7	10.3	-0.07	0.06	0.09	3	0.40	0.02	0.11	3	0.17	0.09	0.12	0.57	0.95	3.98	0.24	0.60
181.74	0.8	6.8	6.4	4.8	11.4	6.0	2.7	3.8	13.4	-0.29	0.12	0.12	3	0.48	0.02	0.11	3	0.17	0.08	0.11	0.43	0.80	3.52	0.23	0.54
182.34	0.9	7.1	4.3	1.9	6.8	2.1	1.8	1.5	7.7									0.15	0.07	0.10	0.40	0.73	3.76	0.19	0.56
182.42	1.0	7.2	4.6	2.2	8.1	2.2	1.8	1.6	9.1									0.16	0.08	0.10	0.37	0.71	3.81	0.19	0.52
187.10	0.9	6.6	3.3	1.9	1.5	2.1	1.4	1.6	1.8									0.16	0.09	0.11	0.33	0.70	3.43	0.20	0.47
187.20	0.8	6.6	3.2	2.1	1.0	2.6	1.4	1.7	1.3									0.15	0.08	0.09	0.46	0.78	3.45	0.23	0.59
Solberga #1 - Kallholn Fm.																									
60.81	4.1	4.2	7.2	17.8	9.8	4.3	4.9	22.7	18.7	-0.25	0.05	0.09	3	0.57	0.10	0.11	3	0.13	0.05	0.04	1.70	1.93	3.31	0.58	0.88
60.81rpt													3	0.56	0.04	0.11	3								
60.90	3.1	3.7	5.4	6.9	5.0	2.2	4.2	10.1	11.0	-0.34	0.06	0.09	3	0.86	0.05	0.11	3	0.11	0.05	0.04	1.28	1.48	2.56	0.58	0.86
61.46	2.9	6.9	9.9	4.0	7.9	1.4	4.1	3.1	9.2	-0.23	0.05	0.09	3	0.67	0.00	0.11	3	0.08	0.06	0.05	0.70	0.88	3.21	0.28	0.79
61.60	6.5	7.3	16.9	44.6	49.9	6.9	6.7	32.7	55.1	-0.01	0.15	0.15	3	0.44	0.03	0.11	3	0.06	0.05	0.04	0.94	1.10	3.23	0.34	0.86
Solberga #1 - the Fjäcka Shale																									
135.01	4.3	5.4	12.6	89.2	55.5	2.9	6.8	89.4	83.4	-0.13	0.07	0.09	3	0.81	0.03	0.11	3	0.14	0.06	0.06	1.99	2.25	3.91	0.57	0.89
135.01rpt1										-0.14	0.08	0.09	3	0.78	0.08	0.11	3								
135.01rpt2	4.3	5.3	13.1	91.5	59.5	3.1	7.1	91.9	89.7					0.76	0.03	0.11	3						4.10		
135.15	4.6	4.6	12.4	45.1	33.0	2.7	7.7	52.1	57.2	-0.15	0.04	0.09	3	0.66	0.01	0.11	3	0.16	0.07	0.06	2.37	2.66	4.16	0.64	0.89
135.15rpt													3	0.64	0.01	0.11	3								
135.49	8.2	6.5	12.5	34.8	79.2	1.5	5.5	28.9	98.4	-0.20	0.03	0.09	3	0.59	0.05	0.11	3	0.12	0.06	0.06	1.33	1.58	3.77	0.42	0.85
135.56	6.8	6.2	14.3	25.2	56.9	2.1	6.7	21.8	74.0	-0.24	0.07	0.09	3	0.62	0.01	0.11	3	0.12	0.06	0.06	1.37	1.61	3.58	0.45	0.85
137.31	6.8	5.7	13.9	17.1	55.6	2.0	7.0	16.2	78.9	-0.15	0.02	0.09	3	0.42	0.04	0.11	3	0.13	0.06	0.05	1.65	1.90	3.52	0.54	0.87
137.35	4.5	5.3	12.7	14.1	21.9	2.8	6.9	14.2	33.2	-0.21	0.06	0.09	3	0.63	0.03	0.11	3	0.14	0.06	0.06	1.72	2.00	3.67	0.54	0.86
Stumsnäs #1 - the Fjäcka Shale																									
217.55	4.0	4.5	15.7	33.2	21.9	8.3	10.1	39.9	39.4	-0.17	0.09	0.09	3	0.71	0.03	0.11	3	0.14	0.08	0.09	1.17	1.48	3.17	0.47	0.79
217.69	5.6	5.2	15.7	35.3	35.1	6.3	8.7	36.4	54.4	-0.16	0.04	0.09	3	0.58	0.04	0.11	3	0.12	0.07	0.07	1.26	1.52	3.31	0.46	0.83
219.42	4.3	4.2	13.6	69.9	35.1	16.3	9.2	88.5	66.7	0.01	0.05	0.09	3	1.09	0.08	0.11	3	0.11	0.06	0.06	0.98	1.20	2.58	0.47	0.81
219.58	7.7	5.3	16.3	102.0	70.7	13.3	8.9	103.9	108.1	0.07	0.04	0.09	3	0.92	0.05	0.11	3	0.09	0.05	0.05	1.04	1.23	2.99	0.41	0.85
219.74	6.8	5.3	16.6	204.9	58.7	30.1	9.0	206.8	88.9	0.10	0.03	0.09	3	1.24	0.03	0.11	3	0.11	0.06	0.05	1.49	1.72	3.36	0.51	0.87
219.74rpt													3	1.16	0.04	0.11	2								
219.95	6.1	5.7	17.1	226.9	48.5	37.2	8.6	214.4	68.8	0.01	0.03	0.09	3	1.28	0.05	0.11	3	0.10	0.06	0.05	1.65	1.86	3.47	0.54	0.89
220.87	4.6	4.4	13.0	50.3	33.7	10.9	8.5	61.8	62.1	-0.06	0.06	0.09	3	1.00	0.01	0.11	3	0.10	0.06	0.05	1.04	1.25	2.75	0.45	0.83
220.87rpt	4.6	4.3	13.1	50.3	33.3	10.9	8.7	62.4	61.9	-0.02	0.03	0.09	3	1.28	0.07	0.11	3						2.59		
220.96	6.3	5.1	13.1	97.6	59.8	15.5	7.4	103.4	95.1	0.03	0.04	0.09	3	0.87	0.03	0.11	3	0.09	0.05	0.06	1.37	1.57	3.04	0.52	0.87
221.32	4.5	5.0	12.1	73.9	23.8	16.4	6.9	78.8	38.1	-0.06	0.06	0.09	3	0.63	0.01	0.11	3	0.10	0.06	0.05	1.20	1.42	3.19	0.44	0.84
221.44	4.5	5.2	11.3	58.5	32.7	13.0	6.2	60.2	50.4	-0.08	0.11	0.11	3	0.63	0.03	0.11	3	0.10	0.06	0.05	1.25	1.47	3.15	0.47	0.85

[a] TOC = total organic carbon

[b] EF = enrichment factor = (metal / Al)$_{sample}$ / (metal / Al)$_{ave.\ upper\ crust}$. Average upper crust metal values are from McLennan (2001) except for Re (Selby et al., 2007).

[c] U isotope data reported relative to CRM 145.

[d] Reported uncertainty is the 2SD of replicate measurements or 0.09‰, whichever is greater.

[e] Number of MC-ICP-MS analyses of the same sample solution.

[f] Mo isotope data reported relative to NIST SRM 3134 = +0.25‰.

[g] Reported uncertainty is the 2SD of replicate measurements or 0.11‰, whichever is greater.

[h] Fe_{HR} = highly reactive iron = carbonate iron (Fe_{Carb}) + ferric-oxide iron (Fe_{Ox}) + magnetite iron (Fe_{Mag}) + pyrite iron (Fe_{PY}).

[I] Fe_T = total iron

Figure 4

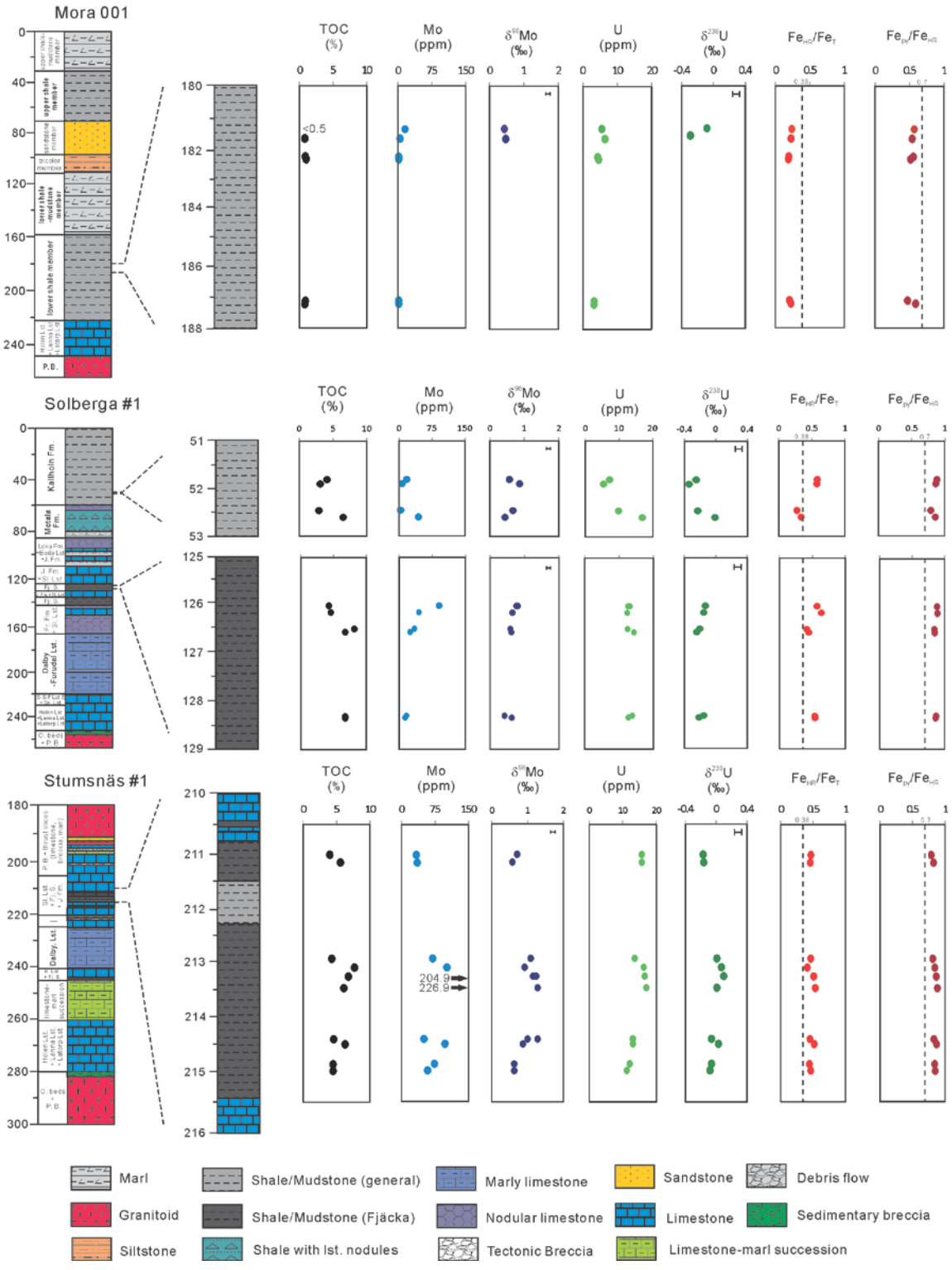

Fig. 4. Geochemical profiles through three drillholes (Mora 001, Solberga #1, and Stumsnäs #1). Stratigraphic columns and formation names of each drillcore are modified from Lehnert et al. (2012, 2013). The error bars in the individual profiles

represent the long-term reproducibility of our secondary standards (~0.09‰ for U and ~0.11‰ for Mo; 2SD). Vertical lines were added to the Fe_{HR}/Fe_T and Fe_{py}/Fe_{HR} columns at values of 0.38 and 0.70, respectively. Fe_{HR}/Fe_T > 0.38 and < 0.22 typically represent anoxic and oxygenated bottom water conditions, respectively. When Fe_{HR}/Fe_T is over 0.38, Fe_{py}/Fe_{HR} can further be used to identify euxinic (>0.7) or ferruginous (<0.7) conditions. Rock properties are beneath the geochemical profiles. ***J. Fm.= Jonstorp Formation; Sl. Lst.= Slandrom Limestone; Fj. S. = Fjäcka Shale; Fr. Fm.= Freberga Formation; S-S-F Lst.E= Skärlöv-Seby-Folkslunda Limestone equivalents; Se. Lst.= Segerstad Limestone; K. Lst.= Kullsberg Limestone; P. B. = Precambrian basement; O. beds = Obolus beds; "—" = shale + debris flow + compact limestone.***

The occurrence of high Mo/U ratios (average = 5.1) in the Fjäcka Shale, which in some cases exceeds three times the modern seawater molar Mo/U ratio, indicates no more than a moderately restricted basin where Mo removal to the euxinic sediments occurred at a faster rate compared with U (Fig. 5b) (Algeo and Tribovillard, 2009). High accumulation rates of Mo in euxinic sediments may also be caused by the operation of a Fe-Mn particulate shuttle that helps promote more efficient uptake of Mo relative to U into sediments deposited from euxinic bottom water conditions similar to that observed in the Cariaco Basin (Algeo and Tribovillard, 2009). These interpretations are consistent with the high Mo/Re ratios (average = 1.7) of the Fjäcka Shale, which fluctuate around the molar Mo/Re ratios of modern seawater (Fig. 5c).

The Mo/TOC ratios in ORMs are found to scale with dissolved Mo concentrations in euxinic bottom waters (Algeo and Lyons, 2006). Specifically, low Mo/TOC ratios were observed in highly restricted basins like the Black Sea due to high Mo removal rates to sediments and slow Mo recharge rates from the open ocean (Algeo and Lyons, 2006). Hence, the relatively high Mo/TOC ratios of the Fjäcka Shale (average: 13.5 ppm/wt%), which are generally intermediate between that of modern euxinic sediments in the

Cariaco Basin (25 ± 5 ppm/wt%) and Framvaren Fjord (9 ± 2 ppm/wt%), suggests moderate basin restriction (Fig. 6a) (Algeo and Lyons, 2006). In contrast, low Mo/U ratios (Algeo and Tribovillard, 2009) and low Mo/TOC ratios (Algeo and Lyons, 2006) are observed in a strongly restricted basin like the Black Sea. However, the correlation between Mo and TOC contents is poor (R^2 = 0.04), as is the correlation between U and TOC contents (R^2 = 0.16) in the Fjäcka Shale (Fig. 6). By contrast, Re and TOC are well-correlated in the Fjäcka Shale (R^2 = 0.93 if sample 135.01 m is excluded).

Compared with the Fjäcka Shale, the black shales of the Kallholn Formation in drillcore Solberga #1 have a relatively lower TOC content with an average of 4.2% (Table 1 and Fig. 4). Positive correlations between trace metals (Mo, U, Re) and TOC are observed for black shales of the Kallholn Formation (Fig. 6). The two stratigraphically highest samples have high Fe_{HR}/Fe_T (>0.38) and Fe_{py}/Fe_{HR} (>0.8), which indicate deposition from euxinic bottom waters (Fig. 4). However, the two stratigraphically lower samples have intermediate Fe_{HR}/Fe_T (0.28−0.34) and high Fe_{py}/Fe_{HR} (0.86−0.89) (Fig. 4). The U (5.4−16.9 ppm), Mo (4.0−44.6 ppm), and Re (5.0−49.9 ppb) concentrations and EFs span a large range (Table 1 and Fig. 4). Specifically, the two stratigraphically higher samples, identified as being deposited from euxinic bottom waters by Fe speciation, have intermediate trace metal EFs (U: 4.24−4.95; Mo: 10.12−22.72; Re: 10.96−18.69) (Table 1 and Fig. 4). The stratigraphically lower sample at 61.60 m has intermediate Fe_{HR}/Fe_T (0.34) and high Fe_{py}/Fe_{HR} (0.86), but the highest trace metal EFs (U: 6.67; Mo: 32.74; Re: 55.06), which also suggests deposition from euxinic waters (Table 1 and Fig. 4).

Figure 5

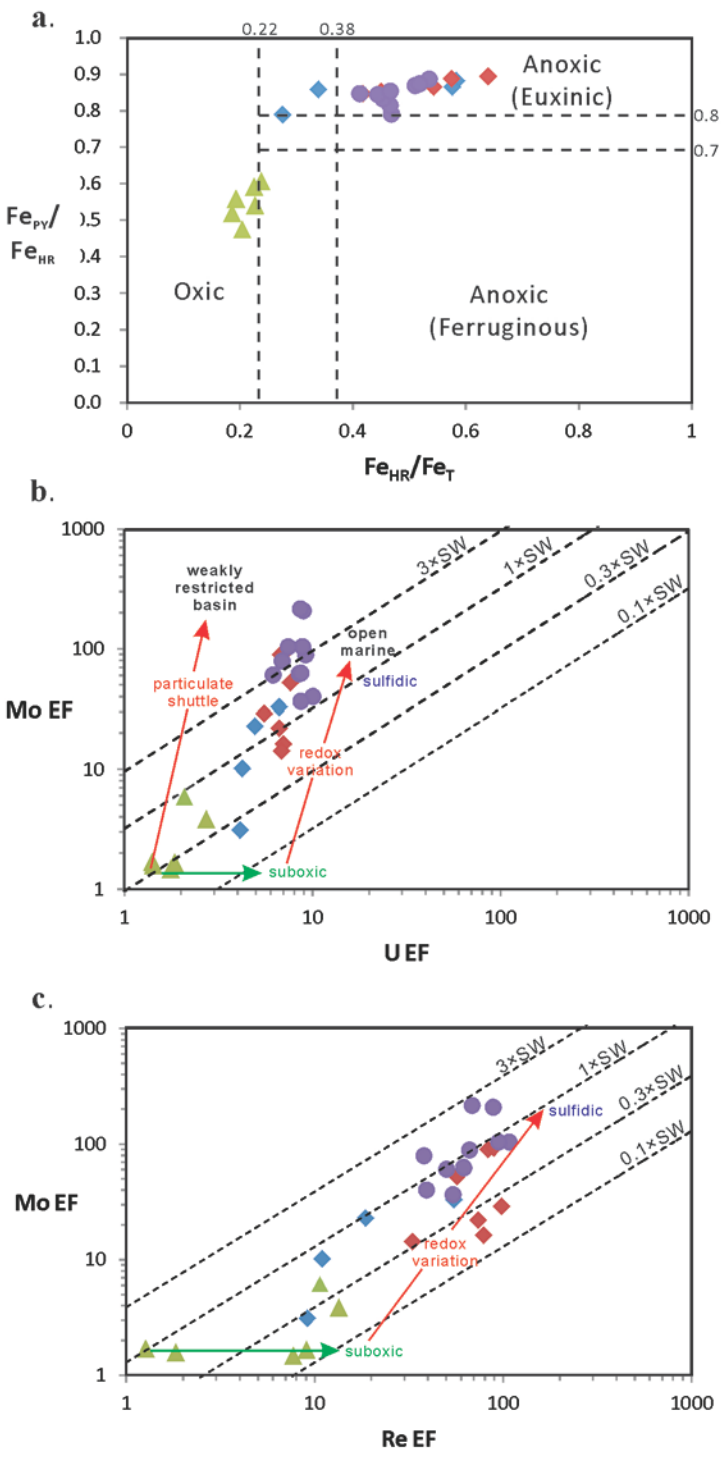
a.
0.22
0.38
Anoxic
(Euxinic)
0.8
0.7
Oxic
Anoxic
(Ferruginous)
Fe_PY/
Fe_HR
Fe_HR/Fe_T
b.
weakly
restricted
basin
open
marine
particulate
shuttle
sulfidic
redox
variation
suboxic
3×SW
1×SW
0.3×SW
0.1×SW
Mo EF
U EF
c.
sulfidic
redox
variation
suboxic
3×SW
1×SW
0.3×SW
0.1×SW
Mo EF
Re EF

Fig. 5. (preceding page) Geochemical diagrams showing a) Fe_{py}/Fe_{HR} versus Fe_{HR}/Fe_T, b) Mo EF versus U EF, c) Mo EF versus Re EF. Dashed lines in a) are used to clarify different bottom water conditions (see details in text). Dashed lines in b) and c) present the molar Mo/U (Algeo and Tribovillard, 2009) and Mo/Re (Crusius et al., 1996) ratios of modern seawater (1 × SW), respectively, and their corresponding fractions of modern seawater (0.1 × SW, 0.3 × SW, and 3 × SW). Enrichment patterns and corresponding controls in b) are illustrated following Algeo and Tribovillard (2009). Re has similar behavior as U (but Re is more sensitive to redox changes), suggesting the general enrichment patterns and redox controls on the two metals are similar (Morford and Emerson, 1999). Hence, similar patterns and controls are plotted in c). ***Green triangles = gray shales [upper Kallholn Formation equivalent] (Mora 001); blue diamonds = Kallholn Formation (Solberga #1); red diamonds = Fjäcka Shale (Solberga #1); purple circles = Fjäcka Shale (Stumsnäs #1).***

On the contrary, the stratigraphically lowest sample at 61.46 m was likely deposited under oxygenated conditions, as indicated by the lowest Fe_{HR}/Fe_T (0.28) and trace metal EFs (U: 4.12; Mo: 3.10; Re: 9.16) in this sample (Table 1 and Fig. 4). These observations are consistent with the range in Mo/U and Mo/Re ratios (Fig. 5). Hence, the local paleoredox conditions during deposition of the Kallholn Formation were not uniform. Based on the Fe speciation and trace metal records, a transiently euxinic and oxygenated depositional environment (where the chemocline fluctuated around the sediment/water interface) is inferred for the Kallholn Formation.

Compared with the black shales of the Fjäcka Shale and Kallholn Formation, the gray shales in drill core Mora 001 have the lowest TOC content (≤ 1.0%) and low U (3.2−6.4 ppm), Mo (1.9−7.4 ppm), and Re (1.0−11.4 ppb) concentrations (Table 1 and Fig. 4). Low Mo EFs (1−6), together with low U EFs (1−3) and low to mild Re EFs (1−13), clearly point to deposition from oxic to suboxic bottom waters, which is consistent with low Fe_{HR}/Fe_T (0.19−0.24) and Fe_{py}/Fe_{HR} (0.47−0.60) ratios (Fig. 5) (Algeo and Tribovillard, 2009).

Figure 6

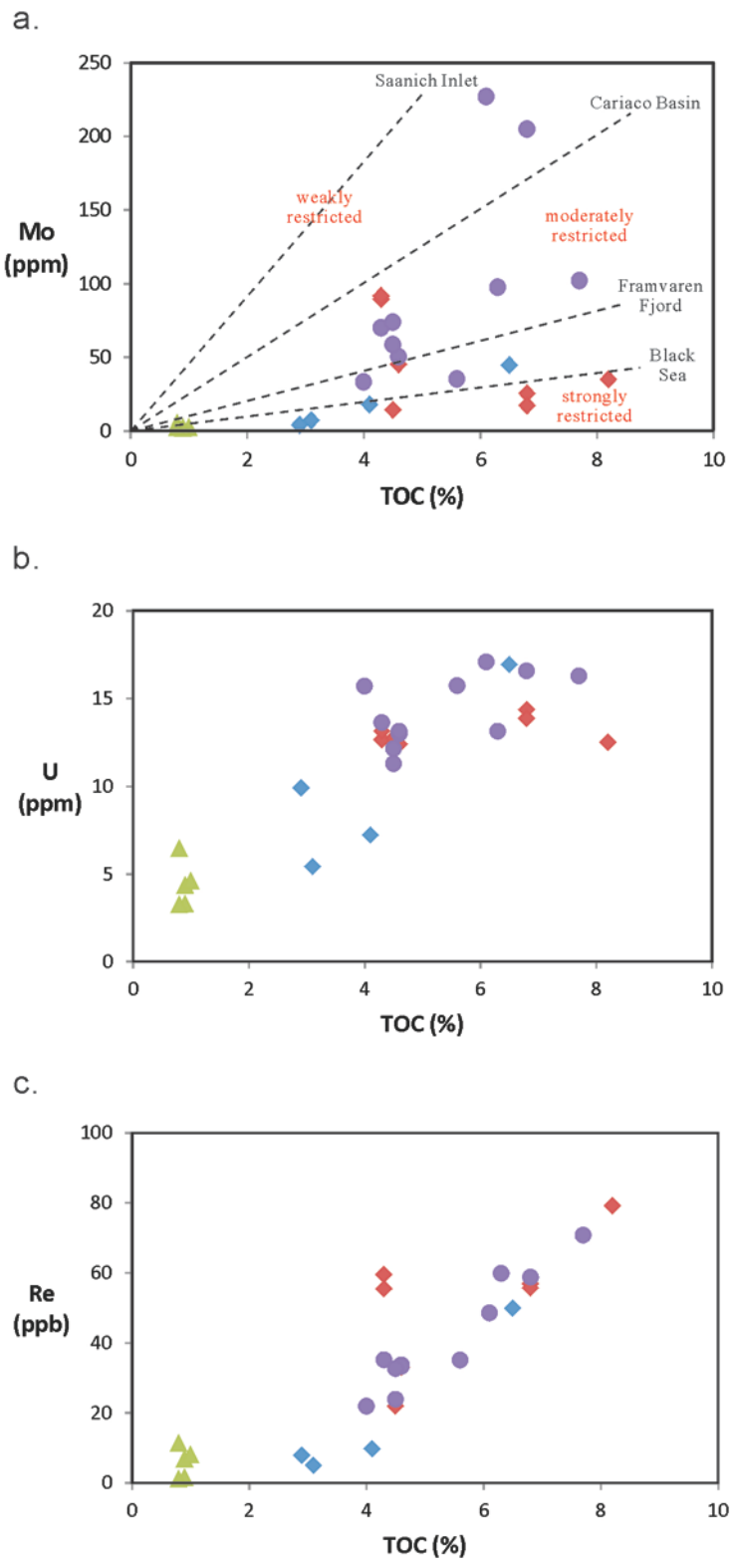
a.
Mo (ppm)
TOC (%)
Saanich Inlet
Cariaco Basin
Framvaren Fjord
Black Sea
weakly restricted
moderately restricted
strongly restricted
b.
U (ppm)
TOC (%)
c.
Re (ppb)
TOC (%)

Fig. 6. (preceding page) Geochemical diagrams showing trace metal concentrations versus TOC; a) Mo vs TOC, b) U vs TOC, and c) Re vs TOC. Dashed lines in a) represent regression slopes for four modern anoxic basins from Algeo and Lyons (2006) (Saanich Inlet: 45 ± 5; Cariaco Basin: 25 ± 5; Framvaren Fjord: 9 ± 2; Black Sea: 4.5 ± 1; in ppm/wt%). ***Green triangles = gray shales [upper Kallholn Formation equivalent] (Mora 001); blue diamonds = Kallholn Formation (Solberga #1); red diamonds = Fjäcka Shale (Solberga #1); purple circles = Fjäcka Shale (Stumsnäs #1).***

Hence, there are three major observations from the TOC, Fe speciation, and trace metal data: 1) the Fjäcka Shale in Stumsnäs #1 and Solberga #1 was deposited under euxinic bottom water conditions; 2) the Kallholn Formation in Solberga #1 represents an intermediate redox state (fluctuations between euxinic and oxygenated bottom waters); and 3) the gray shales in Mora 001, which are equivalent to the upper Kallholn Formation, were deposited in an oxic to suboxic environment.

4.2. Uranium and molybdenum isotope analyses

The δ^{98}Mo values generally increase with increasing Mo EF for the Fjäcka Shale (R^2 = 0.61), whereas the Kallholn Formation black and gray shales display no correlation (R^2 = 0.05) (Fig. 7a). A weak positive correlation between δ^{238}U and U EF is observed for the Fjäcka Shale (R^2 = 0.25), and no correlation is observed for the Kallholn Formation black and gray shales (R^2 = 0.08) (Fig. 7b). Further, δ^{238}U and δ^{98}Mo exhibit a moderately positive correlation for the Fjäcka Shale (R^2 = 0.62), but a moderately negative correlation for Kallholn Formation black and gray shales (R^2 = 0.52) (Fig. 7c).

Figure 7

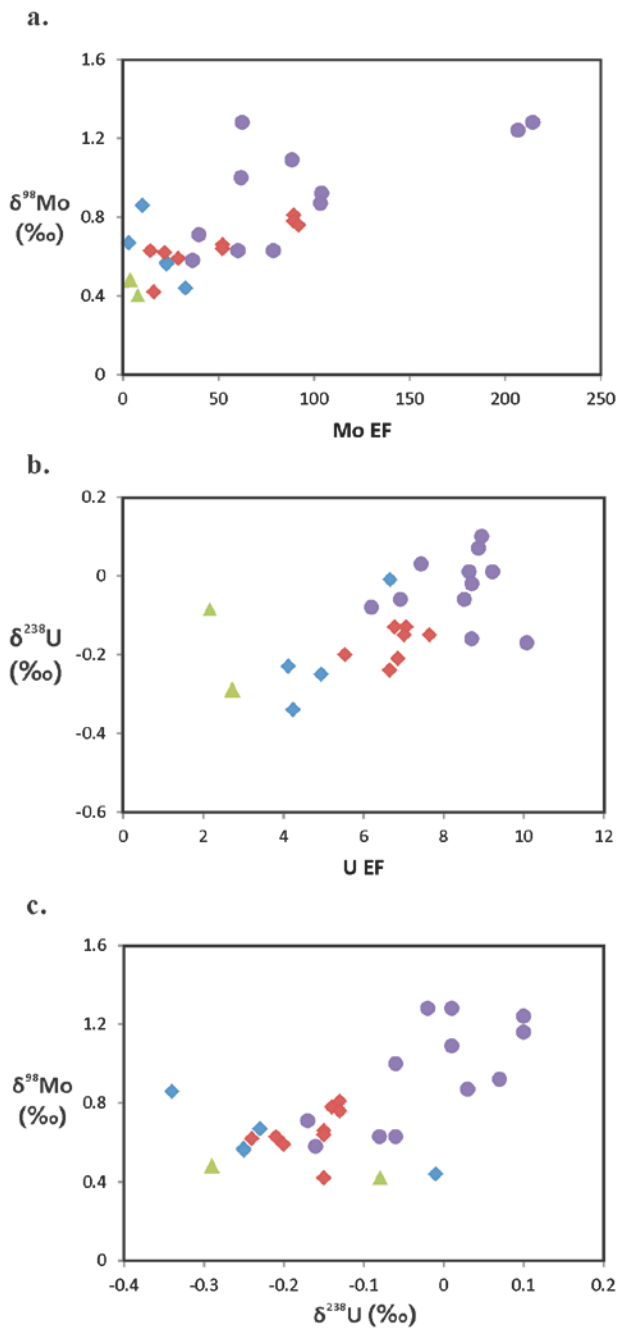

Fig. 7. Geochemical diagrams showing a) δ^{98}Mo versus Mo EF, b) δ^{238}U versus U EF, and c) δ^{98}Mo versus δ^{238}U (see details in text). ***Green triangles = gray shales [upper Kallholn Formation equivalent] (Mora 001); blue diamonds = Kallholn Formation (Solberga #1); red diamonds = Fjäcka Shale (Solberga #1); purple circles = Fjäcka Shale (Stumsnäs #1).***

The $\delta^{238}U$ and $\delta^{98}Mo$ of the Fjäcka Shale range from −0.24‰ to 0.10‰ and from 0.42‰ to 1.28‰, respectively (Table 1). A stratigraphic trend is observed in Stumsnäs #1. Specifically, the central Fjäcka Shale in Stumsnäs #1, which has the highest Mo (> 100 ppm), U (> 16 ppm), and Re (> 48 ppb) concentrations, also yields the highest $\delta^{238}U$ (0.01‰ to 0.10‰) and $\delta^{98}Mo$ (0.92‰ to 1.28‰). On the contrary, the overlying and underlying shales in this drillcore exhibit relatively lower $\delta^{238}U$ (top: −0.17‰ to 0.01‰; bottom: −0.08‰ to 0.03‰) and $\delta^{98}Mo$ (top: 0.58‰ to 1.09‰; bottom: 0.63‰ to 1.28‰). No obvious trend is observed for the Fjäcka Shale in Solberga #1 (Fig. 4). The black shales of the Kallholn Formation in Solberga #1 yield generally lower $\delta^{238}U$ (−0.34‰ to −0.10‰) and $\delta^{98}Mo$ (0.44‰ to 0.86‰) compared with the Fjäcka Shale. A similar observation can be made for two gray shales of the uppermost Kallholn Formation ($\delta^{238}U$: −0.29 to −0.07‰; $\delta^{98}Mo$: 0.40 to 0.48‰) (Table 1).

Hence, two main observations can be derived from the U and Mo isotope data: 1) generally higher Mo and U isotope compositions, and higher Mo, U, and Re concentrations are observed in the euxinic Fjäcka Shale; and 2) the Kallholn Formation yields generally lower Mo and U isotope compositions, and lower Mo, U, and Re concentrations.

5. DISCUSSION

5.1. Suitability of each formation for inferring global ocean redox conditions

Shales deposited under euxinic conditions have the most opportunity to provide insights on global ocean redox conditions using Mo and U concentrations and isotope

compositions. Based on Fe speciation and trace element concentrations, the grey shales (equivalent to the upper Kallholn Formation) and the black shales of the Kallholn Formation were deposited under oxic and transiently euxinic/oxygenated bottom water conditions, respectively. A switch from euxinic conditions to oxygenated conditions can cause re-mobilization and re-deposition of redox-sensitive trace metals at deeper depths within sediments, thus obscuring the original depositional trends (Morford and Emerson, 1999; Morford et al., 2005). This implies that the gray shales and the black shales of the Kallholn Formation are not suitable for inferring global ocean redox conditions. On the contrary, the same paleoredox proxies suggest a persistently euxinic depositional environment for the Fjäcka Shale. Hence, U and Mo concentrations and isotope compositions preserved in the late Katian euxinic Fjäcka Shale are the main focus of efforts to infer global ocean redox conditions in the following discussion.

The scattered relationship between Mo and TOC contents in the Fjäcka Shale (R^2 = 0.04) may suggest the occurrence of post-depositional disturbance (Fig. 6a). Similarly, a poor correlation is observed between U and TOC contents (R^2 = 0.16) (Fig. 6b). The weak correlation between U and TOC contents is expected for ORMs deposited under euxinic conditions because U is not directly associated with organic matter in ORMs but rather is found in authigenic phases like UO_2 (Algeo and Maynard, 2004; Tribovillard et al., 2006). However, the poor correlation between Mo and TOC contents deviates from the strong correlations typically observed for sediments deposited in modern euxinic basins (Algeo and Lyons, 2006). The Re and TOC contents show a much stronger positive correlation (R^2 = 0.44). If sample 135.01 m with high Re but low TOC is excluded, the correlation between Re and TOC contents in the Fjäcka Shale is high (R^2 =

0.93) (Fig. 6c). This observation implies that Re in the Fjäcka Shale is directly derived from seawater (e.g., Anbar et al., 2007), suggesting no post-depositional disturbance to the Fjäcka Shale. The reason for the poor Mo-TOC correlation in the Fjäcka Shale is not known, but may relate to water chemistry. Regardless, the elevated Mo/TOC ratios for many Fjäcka Shale samples point to large amounts of dissolved Mo in the overlying bottom waters, thus suggesting that the degree of basin restriction was not strong (cf. Algeo and Lyons, 2006).

The ORMs of the Fjäcka Shale in Solberga #1 and Stumsnäs #1 have some similarities and differences in geochemical characteristics (Table 1). The average and standard deviation of each type of geochemical data is summarized in Table 2. The TOC contents, Fe speciation, and U and Re concentrations of the Fjäcka Shale from the two drillcores overlap significantly. The biggest differences are observed for Mo concentrations, and U and Mo isotope compositions, which are all higher in Stumsnäs #1. The Fjäcka Shale in Stumsnäs #1 has much higher Mo concentrations compared with that in Solberga #1, raising the possibly of stronger euxinic bottom water conditions at the Stumsnäs #1 locality. Smaller Mo enrichments in the Fjäcka Shale from Solberga #1 may be caused by relatively less H_2S in water column or a faster sedimentation rate at that locality. Although Fe speciation indicates euxinic conditions for the Fjäcka Shale, this technique is not able to differentiate H_2S levels in bottom waters. The relatively deeper burial depth of the Fjäcka Shale in Stumsnäs #1 suggests a deeper depositional environment compared with Solberga #1.

Table 2. Comparison of geochemical data among rock units from each drill core (ave = average)

	TOC (ave, *1SD*)	U (ave, *1SD*) (ppm)	Mo (ave, *1SD*) (ppm)	Re (ave, *1SD*) (ppb)	U EF (ave, *1SD*)	Mo EF (ave, *1SD*)	Re EF (ave, *1SD*)	Mo/TOC (ave, *1SD*) (ppm/%)	$\delta^{238}U$ (ave, *1SD*) (‰)	$\delta^{98}Mo$ (ave, *1SD*) (‰)	Fe_{HR}/Fe_T (ave, *1SD*)	Fe_{PY}/Fe_{HR} (ave, *1SD*)
Fjäcka Shale	5.6, *1.3*	13.8, *1.7*	73.3, *58.7*	45.3, *17.3*	7.8, *1.2*	76.2, *56.9*	69.4, *21.9*	13.5, *9.4*	- 0.09, *0.10*	0.82, *0.26*	0.49, *0.06*	0.85, *0.03*
Fjäcka Shale (Stumsnäs #1)	5.4, *1.3*	14.3, 2.0	91.2, *65.7*	41.2, *15.9*	8.4, *1.1*	96.1, *60.9*	66.7, *22.5*	16.2, *9.3*	- 0.03, *0.09*	0.95, *0.27*	0.47, *0.04*	0.84, *0.03*
Fjäcka Shale (Solberga #1)	5.6, *1.6*	13.1, *0.8*	45.3, *32.5*	51.7, *18.7*	6.8, *0.6*	44.9, *33.7*	73.5, *22.0*	9.4, *8.3*	- 0.17, *0.04*	0.66, *0.12*	0.53, *0.08*	0.87, *0.02*
Kallholn Formation	4.2, *1.7*	9.9, *5.1*	18.3, *18.5*	18.2, *21.3*	5.0, *1.2*	17.2, *13.2*	23.5, *21.5*	3.7, *2.4*	- 0.21, *0.14*	0.62, *0.16*	0.44, *0.16*	0.85, *0.04*
Gray shale (equivalent to upper Kallholn Formation)	0.9, *0.1*	4.5, *1.2*	3.4, *2.3*	6.3, *4.2*	1.9, *0.5*	2.6, *1.8*	7.3, *4.8*	3.0, *1.7*	- 0.18, *0.16*	0.44, *0.06*	0.21, *0.02*	0.55, *0.05*

Hence, the geological and geochemical observations for the Fjäcka Shale from Stumsnäs #1 suggest that this locality represents the most euxinic and deepest water depositional environment. Hence, the ORMs from this drill core are the most suitable for inferring global ocean redox conditions when using Mo isotopes as a global ocean paleoredox proxy. Although heavier U isotope compositions are also observed in Stumsnäs #1, the U isotope composition of euxinic sediments in modern anoxic basins does not appear to have a positive correlation with the amount of dissolved hydrogen sulfide in bottom waters (Andersen et al., 2014; Holmden et al., 2015).

High Mo/U ratios of the Fjäcka Shale from Stumsnäs #1, in some cases exceeding three times the modern seawater molar Mo/U ratio, indicates the potential operation of a particulate shuttle as observed in the modern Cariaco Basin (Fig. 5b) (Algeo and Tribovillard, 2009). Besides enhanced Mo enrichments, the particulate shuttle will lead to sediments enriched in isotopically light Mo because Fe-Mn oxides have low δ^{98}Mo, and the reductive dissolution of Fe-Mn oxides in sediments enables this isotopically light Mo to be recaptured by sulfides and organic matter in the sediments (e.g., Herrmann et al., 2012). In this scenario, the Fjäcka Shale samples with the highest Mo/U ratios should generally preserve lower δ^{98}Mo than the units with lower Mo/U ratios. In contrast, the highest δ^{98}Mo accompanies high Mo/U ratios in the Fjäcka Shale, implying that the particulate shuttle is not the cause of the low Mo isotope compositions. In addition, a model of enrichment patterns and controls on $(Mo/U)_{auth}$ ratios in organic-rich sediments based on modern environments revealed a much steeper slope of $(Mo/U)_{auth}$ associated with operation of a particulate shuttle (Algeo and Tribovillard, 2009). However, the slope of the Fjäcka Shale is more similar to the slope associated with redox variations in the

water column, thus indicating weak or negligible operation of the particulate shuttle in the local depositional environment (Fig. 5b). This interpretation is consistent with observations from Mo/Re ratios (Fig. 5c), and further supported by positive correlation between Mo concentrations and δ^{98}Mo for the Fjäcka Shale (Fig. 7a).

5.2. A relatively oxygenated Katian ocean inferred from U isotope data

5.2.1. U isotope evidence for appreciable oxygenation in the late Katian ocean

Uranium appears in minerals and rocks in both reduced U(IV) and oxidized U(VI). In modern oxygenated seawater, uranium is highly soluble as U(VI) and exhibits conservative behavior with a long residence time (~ 400-500 kyr) in the oceans (Ku et al., 1977; Dunk et al., 2002). The U(VI) species combine with oxygen to form the uranyl cation ($[UO_2]^{2+}$), which in turn usually complexes with carbonate to form uranyl carbonate ($UO_2[CO_3]_3^{4-}$; Langmuir, 1978). In contrast, U is reduced from soluble U(VI) to insoluble U(IV) and removed into organic-rich sediments in an anoxic environment (Anderson et al., 1987; Barnes and Cochran, 1990; Morford and Emerson, 1999; McManus et al., 2006). In anoxic settings, U still exists as soluble U(VI) even in the deep part of the Black Sea where there is a high $H_2S_{(aq)}$ concentration, indicating that U removal occurs below the sediment-water interface (Anderson, 1987; Anderson et al., 1989). The main U removal process is diffusion of uranyl carbonate from seawater, reduction to U(IV) at or below the depth for the reduction of Fe(III) to Fe(II) in sediments, and subsequently adsorption or precipitation as UO_2 (e.g., Anderson et al., 1989). Removal of U from pore waters to sediments is likely associated with organic matter, namely the formation of organometallic ligands, under anoxic/non-sulfidic conditions

(Anderson et al., 1989; Dunk et al., 2002). In euxinic conditions, direct precipitation of authigenic U phases is favored over an association with organic matter (Algeo and Maynard, 2004; Tribovillard et al., 2006).

With regards to oceanic inputs, U is primarily derived from the oxidative weathering of continental crust, and subsequent transport of dissolved U(VI) by rivers to the oceans (Morford and Emerson, 1999; Dunk et al., 2002; Partin et al., 2013b). Biogenic carbonates and sediments deposited beneath anoxic and suboxic waters are the three major sinks for U. Hydrothermally altered oceanic crust and sediments deposited under oxygenated bottom waters are minor oceanic U sinks (Morford and Emerson, 1999; Dunk et al., 2002; Partin et al., 2013b).

The U isotope system has been suggested to be a promising oceanic paleoredox proxy with great potential based on several recent studies of carbonates (Stirling et al., 2007; Weyer et al., 2008; Brennecka et al., 2011a; Romaniello et al., 2013), Fe-Mn crusts (Stirling et al., 2007; Weyer et al., 2008; Goto et al., 2014), and recent and past ORMs (Stirling et al., 2007; Weyer et al., 2008; Montoya-Pino et al., 2010; Asael et al., 2013; Kendall et al., 2013, 2015; Andersen et al., 2014; Holmden et al., 2015; Noordmann et al., 2015). Modern well-oxygenated seawater has a $\delta^{238}U$ of −0.41 ± 0.03‰ (Stirling et al., 2007; Weyer et al., 2008; Tissot and Dauphas, 2015). The new average $\delta^{238}U$ of the upper crust (−0.29 ± 0.03‰; Tissot and Dauphas, 2015) is slightly heavier than that of modern seawater by ~0.1‰, which is consistent with previous estimations (−0.31 ± 0.14‰) based on twenty-four granitoids (Telus et al., 2012) and four basalts (Weyer et al., 2008). Rivers have an average $\delta^{238}U$ of about −0.3‰ (−0.34‰ from Andersen et al., 2016; −0.24‰

from Noordmann et al., 2010, 2011; Tissot and Dauphas, 2015), which is close to the average of the upper crust.

In anoxic environments, a large U isotope fractionation is often observed during the reduction and precipitation of U in the sediments (Stirling et al., 2007; Weyer et al., 2008). It can be explained by the mass-independent, volume-dependent mechanism termed the nuclear field shift, which will result in the preferential removal of heavier U isotopes from seawater to sediments (Biegeleisen, 1996; Schauble, 2007). Recent ORMs from Black Sea Unit I, deposited under strongly euxinic conditions ($H_2S_{(aq)} > 11$ μM), have an average $\delta^{238}U$ value near 0‰ (Weyer et al., 2008; Montoya-Pino et al., 2010), which is about 0.4‰ higher compared with that of modern global seawater (−0.41 ± 0.03‰). However, the magnitude of U isotope fractionation in the Black Sea can only be regarded as a minimum for U(VI) reduction and removal to sediments due to the strong basin restriction of the Black Sea (Anderson et al., 1989). A conceptual model combining the extent of U removal from a water column to the U isotope composition of euxinic sediments was proposed by Andersen et al. (2014), who suggested that a U isotope fractionation of 0.6‰ occurs between seawater and open ocean euxinic sediments. This fractionation factor has been confirmed by the study of modern euxinic basins, including the Saanich Inlet (Holmden et al., 2015), Cariaco Basin (Andersen et al., 2014), Baltic Sea (Noordmann et al., 2015), and Kyllaren Fjord (Noordmann et al., 2015). Accordingly, the representative authigenic $\delta^{238}U$ of modern open ocean euxinic sediments is 0.2‰ whereas lower values are expected in euxinic sediments deposited in strongly restricted marine basins like the Black Sea. Hence, an average global U isotope fractionation of 0.5‰

between seawater and euxinic sediments is an appropriate estimate when considering the variable degree of anoxic basin restriction around the world.

In other marine U sinks, samples from the Peru continental margin overlying suboxic bottom waters yield a slightly heavier U isotope value (−0.28 ± 0.19‰) than modern seawater (Weyer et al., 2008). The $\delta^{238}U$ of Fe-Mn crusts from the Atlantic and Pacific oceans overlying well-oxygenated bottom waters are even lighter, with an average value of −0.59 ± 0.08‰ (Weyer et al., 2008; Brennecka et al., 2011b; −0.65 ± 0.05‰ for the Pacific Ocean from Goto et al., 2014). In this case, when U is adsorbed onto Mn-oxyhydroxide, a different isotope fractionation mechanism occurs, which was proposed to be caused by the differences in the U-O coordination shell between dissolved and adsorbed U (Brennecka et al., 2011b). Primary carbonate precipitates have $\delta^{238}U$ (average: −0.37 ± 0.12‰) that is indistinguishable from global seawater (−0.41 ± 0.03‰) regardless of biological or mineralogical origin, which indicates the ability of such precipitates for directly recording seawater U isotope compositions (Romaniello et al., 2013). However, the $\delta^{238}U$ of shallow bulk carbonates exhibit a U isotope fractionation of 0.2-0.4‰ compared with that of modern seawater, with values ranging from −0.2‰ to 0.0‰, implying an influence of sulfidic pore waters in bulk carbonate sediments on U reduction and deposition (Romaniello et al., 2013).

The well-oxygenated modern ocean, which has a limited distribution of suboxic and anoxic/euxinic environments, has a slightly lighter $\delta^{238}U$ (−0.41 ± 0.03‰) than the rivers (average: −0.3‰), consistent with the small U isotope fractionation (0.18–0.24‰) associated with U removal to Fe-Mn oxides in oxygenated environments. In comparison, an expansion of ocean anoxia will increase the extent of preferential removal of

isotopically heavier U from seawater to anoxic sediments, thus causing lighter $\delta^{238}U$ in the global ocean (Weyer et al., 2008; Montoya-Pino et al., 2010; Brennecka et al., 2011a). Therefore, ancient ORMs deposited during times of expanded ocean anoxia compared with today will have lower $\delta^{238}U$ once seawater $\delta^{238}U$ has shifted to lower values. Hence, lower U isotope compositions in ancient ORM should point to more widespread ocean anoxia, whereas higher U isotope compositions indicate an extensively oxygenated ocean.

It should be noted that the magnitude of authigenic U enrichments in the Fjäcka Shale is lower compared with authigenic Mo enrichments, indicating that the U isotope data is more influenced by the detrital component in these rocks. Holmden et al. (2015) proposed that detrital $\delta^{238}U$ may have a much lower value (−0.83 ± 0.12‰) in Saanich Inlet sediments compared with the average upper continental crust as a result of preferential release of ^{238}U into solution during weathering (−0.29 ± 0.03‰; Tissot and Dauphas, 2015). However, Andersen et al. (2016) suggested limited U isotope fractionation from the upper continental crust during weathering. Hence, a range of detrital $\delta^{238}U$ (−0.3‰ to −0.8‰) is reasonable to use since it is not clear what $\delta^{238}U$ is representative for all detrital materials. A correction for detrital U composition can be made using the following equation (Asael et al., 2013):

$$\delta^{238}U_{auth} = \delta^{238}U_{sam} - (Al/U)_{sam} \times \{(\delta^{238}U_{det} - \delta^{238}U_{sam}) / [(Al/U)_{det} - (Al/U)_{sam}]\}$$

where “auth”, "sam", and "det" represent authigenic U, sample U, and detrital U, respectively. Detrital Al and U concentrations are assumed to be the average upper continental crust values of 8.04% and 2.8 ppm, respectively (McLennan, 2001). A range of detrital $\delta^{238}U$ (from −0.3‰ to −0.8‰) is used to take into account the possibility of U isotope fractionation during continental weathering (Holmden et al., 2015).

Table 3. Authigenic U isotope compositions of the Fjäcka Shale

Sample	Al (wt%)	U (ppm)	$\delta^{238}U$[a] (‰)	2SD Measured	2SD[b] Reported	n[c]	$\delta^{238}U_{auth}$[d] (‰)	f_{auth}[f] (%)	f_{det}[g] (%)	$\delta^{238}U_{auth}$[d] (‰)	f_{auth}[f] (%)	f_{det}[g] (%)
							$\delta^{238}U_{det}$[e] = -0.3‰			$\delta^{238}U_{det}$[e] = -0.8‰		
Solberga #1 - the Fjäcka Shale												
135.01	5.35	12.6	-0.13	0.07	0.09	3	-0.10	0.85	0.15	-0.01	0.85	0.15
135.01rpt[h]	5.35	12.6	-0.14	0.08	0.09	3	-0.11	0.85	0.15	-0.03	0.85	0.15
135.15	4.65	12.4	-0.15	0.04	0.09	3	-0.13	0.87	0.13	-0.05	0.87	0.13
135.49	6.47	12.5	-0.20	0.03	0.09	3	-0.18	0.82	0.18	-0.07	0.82	0.18
135.56	6.19	14.3	-0.24	0.07	0.09	3	-0.23	0.85	0.15	-0.14	0.85	0.15
137.31	5.67	13.9	-0.15	0.02	0.09	3	-0.13	0.86	0.14	-0.04	0.86	0.14
137.35	5.32	12.7	-0.21	0.06	0.09	3	-0.19	0.85	0.15	-0.11	0.85	0.15
Stumsnäs #1 - the Fjäcka Shale												
217.55	4.47	15.7	-0.17	0.09	0.09	3	-0.16	0.90	0.10	-0.10	0.90	0.10
217.69	5.19	15.7	-0.16	0.04	0.09	3	-0.14	0.89	0.11	-0.08	0.89	0.11
219.42	4.23	13.6	0.01	0.05	0.09	3	0.05	0.89	0.11	0.11	0.89	0.11
219.58	5.26	16.3	0.07	0.04	0.09	3	0.12	0.89	0.11	0.18	0.89	0.11
219.74	5.31	16.6	0.10	0.03	0.09	3	0.15	0.89	0.11	0.21	0.89	0.11
219.95	5.67	17.1	0.01	0.03	0.09	3	0.05	0.88	0.12	0.12	0.88	0.12
220.87	4.37	13.0	-0.06	0.06	0.09	3	-0.03	0.88	0.12	0.04	0.88	0.12
220.87rpt	4.32	13.1	-0.02	0.03	0.09	3	0.02	0.89	0.11	0.08	0.89	0.11
220.96	5.06	13.1	0.03	0.04	0.09	3	0.08	0.87	0.13	0.16	0.87	0.13
221.32	5.03	12.1	-0.06	0.06	0.09	3	-0.02	0.86	0.14	0.06	0.86	0.14
221.44	5.21	11.3	-0.08	0.11	0.11	3	-0.04	0.84	0.16	0.06	0.84	0.16

[a] = U isotope date reported relative to CRM145

[b] = Reported uncertainty is the 2SD of replicate measurements or 0.09‰, whichever is greater

[c] = Number of MC-ICP-MS analyses of the same sample solution

[d] = Authigenic U isotope composition

[e] = Detrital U isotope composition

[f] = Fractions of authigenic U in the sample

[g] = Fractions of detrital U in the sample

[h] = Only U isotope data is reanalyzed for this sample

Although the Fjäcka Shale from Stumsnäs #1 may represent the most euxinic bottom water conditions based on the Mo data, the U isotope compositions of euxinic ORMs are not thought to depend on the amount of aqueous H_2S in the water column (Andersen et al., 2014; Holmden et al., 2015). Hence, we correct the U isotope compositions of the Fjäcka Shale from both drillcores for detrital composition and report an overall average authigenic $\delta^{238}U$ (Table 3). After correction, it is found that detrital U comprises up to 15% of the U in the Fjäcka Shale. The average authigenic $\delta^{238}U$ of the Fjäcka Shale is −0.05 ± 0.11‰ (1SD) and 0.02 ± 0.11‰ (1SD) when using detrital $\delta^{238}U$ values of −0.3‰ and −0.8‰, respectively.

The relatively high authigenic $\delta^{238}U$ of the Fjäcka Shale (−0.05‰ to 0.02‰; or an overall average of ~0‰) is an indicator of a relatively oxygenated ocean prior to the Hirnantian glaciation, based on our understanding of the modern U isotope budget. Applying a U isotope fractionation of 0.5‰ between euxinic sediments (deposited in a moderately restricted basin) and global seawater to the average authigenic $\delta^{238}U$ of the Fjäcka Shale (~0‰), we suggest that the $\delta^{238}U$ of the late Katian ocean was approximately −0.5‰ which is slightly lower than the modern ocean. This interpretation is based on the assumption that the riverine $\delta^{238}U$ during the late Katian was generally similar to the present day (−0.3‰) because ORMs with both high U concentrations and high $\delta^{238}U$ (e.g., late Ediacaran ORMs; Kendall et al., 2015) were possibly exposed at the Earth's surface for weathering during the late Ordovician as they are today. Hence, a small offset of about 0.1‰ between the late Katian ocean (–0.5‰) and the modern ocean (−0.4‰) indicates a relatively well-oxygenated late Katian ocean, though not as well-oxygenated as the modern ocean.

A high average $\delta^{238}U$ (0.24 ± 0.16‰) was reported for most ORMs in Member IV of the late Ediacaran Doushantuo Formation, which is similar to the value of 0.2‰ for modern euxinic ORMs in the open ocean (Andersen et al., 2014; Holmden et al., 2015; Kendall et al., 2015). This observation points to an extent of ocean oxygenation in the late Ediacaran that was probably comparable to the present day (Kendall et al., 2015). However, the deposition of euxinic ORMs deposited (based on Fe/Al values greater than 0.5 and high trace metal concentrations) during Oceanic Anoxic Event 2 (OAE2) in open-ocean settings have an average $\delta^{238}U$ of −0.07‰ ± 0.09‰ (or ≈ −0.05‰) (Montoya-Pino et al., 2010). Applying a 0.6‰ fractionation between seawater and open ocean euxinic

settings, it is suggested that the seawater during OAE2 should have $\delta^{238}U$ of −0.65‰ (= −0.05‰ − 0.6‰), which is significantly less than modern seawater (−0.4‰) and late Katian seawater (–0.5‰). Hence, the intermediate $\delta^{238}U$ values from the Fjäcka Shale indicate that the late Katian ocean is relatively more oxygenated compared with OAE2 but is less oxygenated than the modern ocean and the late Ediacaran ocean.

5.2.2. Quantitative constraints on ocean redox conditions during the late Katian based on U isotopes

5.2.2.1. Uranium isotope mass balance in the modern ocean

Uranium isotope mass balance modeling can be used to estimate the extent of oxygenated and anoxic conditions in the oceans during the late Katian. This method has been used to constrain the extent of ocean anoxia during OAE2 (Montoya-Pino et al., 2010) and the end-Permian mass extinction event (Brennecka et al., 2011a). The U isotope mass balance equation is defined below (Montoya-Pino et al., 2010):

$$\delta^{238}U_{input} = (f_{other} \times \delta^{238}U_{other}) + (f_{anox} \times \delta^{238}U_{anox}),$$

where “input” represents riverine U inputs, “other” represents all other U sinks (oxic, suboxic, and hydrothermal), “anox” represents anoxic and euxinic sinks, “f” represents the fraction of U removed into each corresponding sink, and $f_{other} + f_{anox} = 1$.

It was suggested that the anoxic/euxinic sink accounts for approximately 14% of U removal from the modern ocean (Tissot and Dauphas, 2015). Therefore, other sinks represent 86% of U removal. The average U isotope composition for the riverine input is about −0.3‰ (Noordmann et al., 2010, 2011; Tissot and Dauphas, 2015; Andersen et al., 2016). A U isotope fractionation of 0.4‰ occurs between seawater (–0.4‰) and the

strongly euxinic deep-water sediments of the highly restricted Black Sea (0‰). A U isotope fractionation of 0.6‰ is more likely to occur between modern open ocean euxinic sediments and global seawater, which in turn indicates a $\delta^{238}U$ value of 0.2‰ for such sediments (Andersen et al., 2014; Holmden et al., 2015; Noordmann et al., 2015). Thus, considering the variable degree of basin restriction in anoxic/euxinic settings worldwide, a value of 0.5‰ is an appropriate estimate of the average global U isotope fractionation in anoxic/euxinic environments, resulting in an average $\delta^{238}U$ of 0.1‰ for the anoxic/euxinic sink (Montoya-Pino et al., 2010). Applying these values to the U isotope mass balance equation, all other modern U sinks have an average $\delta^{238}U$ of −0.34‰, which corresponds to a fractionation of ~0.1‰ relative to seawater (Fig. 8A; Weyer et al., 2008).

Figure 8

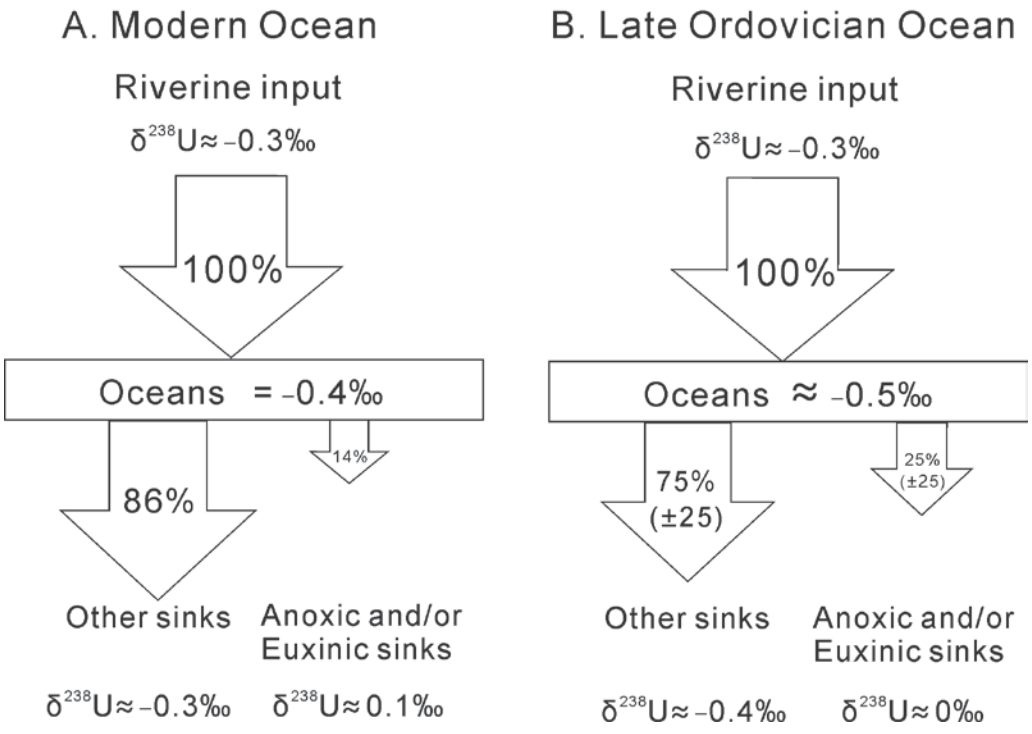

Fig. 8. Uranium isotope mass balance for A) the modern ocean and B) the late Katian ocean, and associated estimates of the anoxic/euxinic sink. Assumptions and calculation methods are described in detail in the text.

5.2.2.2. Uranium isotope mass balance in the late Katian ocean

The U isotope mass balance equation can also be used to estimate the proportion of U that was removed into the two different sinks in the late Ordovician using the modern mass balance as a starting point (Montoya-Pino et al., 2010; Brennecka et al., 2011a). Based on an estimate of 0.5‰ for U isotope fractionation between seawater and the Fjäcka euxinic sediments (authigenic $\delta^{238}U \sim 0‰$) in a moderately restricted basin, it is reasonable to infer that late Katian seawater had a U isotope composition of –0.5‰. It is also appropriate to assign an uncertainty to the late Katian seawater $\delta^{238}U$ to take into account the range of U isotope compositions in the Fjäcka Shale and uncertainty in the magnitude of the U isotope fractionation factor during U removal to euxinic sediments (including uncertainty in the degree of basin restriction). Hence, the $\delta^{238}U$ of late Ordovician Katian seawater is suggested to be –0.5‰ ± 0.1‰. It is assumed that there was a similar U isotope composition for late Katian and modern riverine inputs (–0.3‰) and a constant U isotope fractionation between seawater and the two different sinks (anoxic/euxinic and all other sinks) through time. The latter assumption implies that for late Katian seawater = –0.5‰, the $\delta^{238}U$ of the anoxic/euxinic sink and all other sinks are 0‰ (= –0.5 + 0.5 ‰) and –0.4‰ (= –0.5 + 0.1 ‰), respectively. At the same time, the sum of f_{other} and f_{anox} should equal 100%.

Thus, the calculated fractions of the other sinks and anoxic/euxinic sinks in the late Katian ocean are approximately 75% ± 25% and 25% ± 25%, respectively (Fig. 8B). According to the U isotope mass balance model, the proportion of U removed to

anoxic/euxinic sinks in the late Katian ocean may have been double compared with that of the modern ocean.

This new constraint on the extent of ocean anoxia during the late Katian can be compared with other Phanerozoic oceanic anoxic events studied using U isotopes. It should be noted that seawater $\delta^{238}U$ during OAE2 is −0.65‰ when applying the U isotope fractionation of 0.6‰ (Andersen et al., 2014; Holmden et al., 2015; Noordmann et al., 2015) for the open ocean euxinic ORM analyzed from that time. This is slightly lower than the OAE2 seawater $\delta^{238}U$ of −0.55‰ estimated by Montoya-Pino et al. (2010). In this scenario, the $\delta^{238}U$ of the anoxic/euxinic and the rest of the U sinks are −0.15‰ and −0.55‰, respectively. With the same assumptions for the U isotope mass balance as for the late Katian ocean, the proportion of the anoxic/euxinic sink is 60% ± 25% during OAE2, which is more severe than the previous estimate of 40% ± 25% by Montoya-Pino et al. (2010). Ocean anoxia during the end-Permian mass extinction was modeled using the U isotope compositions of carbonates, which provided an estimate of 60% ± 25% for the proportion of anoxic/euxinic sinks during that time interval (Brennecka et al., 2011a). Thus, the oceans were probably more oxygenated during the late Katian compared with oceans during OAE2 (Montoya-Pino et al., 2010) and the end-Permian mass extinction (Brennecka et al., 2011a) (Fig. 8B).

5.3. Marine redox conditions during the late Katian as inferred from Mo isotopes

Molybdenum is a trace metal with low abundances in the Earth's crust (1.5 ppm; McLennan, 2001). In oxygenated seawater, Mo is conservative with a concentration of 105 nmol/kg (Collier, 1985) and a long residence time of 440 kyr (Miller et al., 2011).

The highly soluble molybdate (MoO_4^{2-}) is the dominant species in oxygenated seawater (Barling et al., 2001). However, in an anoxic environment, Mo is removed into sediments, especially with the occurrence of hydrogen sulfide in bottom waters (e.g., Emerson and Huested, 1991; Helz et al., 1996; Erickson and Helz, 2000). Intermediate thiomolybdate ions (e.g., $MoO_{4-x}S_x^{2-}$) form first before tetrathiomolybdate, and can be the dominant species if the $H_2S_{(aq)}$ concentration is low (Erickson and Helz, 2000; Nägler et al., 2005; Poulson et al., 2006; Siebert et al., 2006; Neubert et al., 2008). A rapid transformation from molybdate (MoO_4^{2-}) to intermediate thiomolybdates to tetrathiomolybdate (MoS_4^{2-}) occurs when $H_2S_{(aq)}$ is greater than 11 μM (Erickson and Helz, 2000). Hence, the efficiency of Mo removal to sediments is the highest in euxinic settings, intermediate in suboxic/anoxic settings with H_2S confined to sediment pore waters, and the lowest in well-oxygenated settings (Scott and Lyons, 2012). The removal process is usually related to Mo sequestration by organic material and solid Fe-S phases (Helz et al., 1996, 2011; Erickson and Helz, 2000; Algeo and Lyons, 2006; Tribovillard et al., 2006; Dahl et al., 2013; Chappaz et al., 2014).

Rivers and low-temperature hydrothermal fluids are the two major sources of Mo to the modern ocean, with rivers accounting for more than 90% of the input flux (e.g., Morford and Emerson, 1999; McManus et al., 2002). Oxic, suboxic to anoxic (H_2S confined to sediment pore waters), and euxinic environments (H_2S in water column) are the three major oceanic sinks of Mo (Arnold et al., 2004; Nägler et al., 2005; Poulson et al., 2006; Siebert et al., 2006; Scott et al., 2008).

The Mo isotope system has been significantly developed and widely used over the past decade to reconstruct global paleoredox conditions and reveal the evolution of ocean

oxygenation through time (e.g., Barling et al., 2001; Siebert et al., 2003, 2006; Arnold et al., 2004; Poulton et al., 2006; Kendall et al., 2009, 2011, 2015; Dahl et al., 2010b; Duan et al., 2010; Herrmann et al., 2012; Zhou et al., 2012, 2015; Chen et al., 2015). The modern ocean has a δ^{98}Mo of 2.34 ± 0.10‰ (Barling et al., 2001; Siebert et al., 2003; Nakagawa et al., 2012; Nägler et al., 2014). Riverine input has various δ^{98}Mo ranging from 0.2 to 2.3‰, with an average value of 0.7‰ (Archer and Vance, 2008). McManus et al. (2002) measured low-temperature hydrothermal fluids from the Juan de Fuca Ridge and got an average δ^{98}Mo of 0.8‰. However, this measurement may not be accurate because the Mo may come from the surrounding bedrocks that the fluid percolated through. Pearce et al. (2010) tested terrestrial hydrothermal spring waters and obtained a δ^{98}Mo of –3.4‰. Thus, the δ^{98}Mo of marine hydrothermal fluid is still not well known.

In well-oxygenated modern seawater, Mo is removed via adsorption to Fe-Mn oxides and crusts (Barling et al., 2001; Siebert et al., 2003; Barling and Anbar, 2004). Lighter Mo isotopes are more likely to be removed into Mn oxyhydroxides compared with relatively heavier Mo isotopes, which makes modern seawater enriched in heavier Mo isotopes (2.34 ± 0.10‰) compared with rivers (average = 0.7‰) (Barling et al., 2001; Siebert et al., 2003; Archer and Vance, 2008). A large Mo isotope fractionation close to 3‰ is observed during this adsorption process, which causes the δ^{98}Mo of Fe-Mn oxides and crusts to be around –0.7‰ (Barling et al., 2001; Siebert et al., 2003; Poulson et al., 2006). This observed fractionation factor (~3‰) is quite similar to the value of 2.7‰ determined by experimental methods (Barling and Anbar, 2004).

In contrast, a much smaller Mo isotope fractionation (0.7‰) is observed in continental margin ORMs deposited in weakly oxygenated ($O_2 \leq 10$ μM) and anoxic

environments where H_2S is restricted to the sediment pore waters, resulting in a δ^{98}Mo of around 1.6‰ (Poulson et al., 2006). Under mildly oxygenated bottom waters (O_2: 10-35 μM) on continental margins, Mo adsorption to Fe-Mn oxides yields a range of δ^{98}Mo from –0.5‰ to 1.3‰ (Siebert et al., 2006; Poulson Brucker et al., 2009), which is intermediate between sediments deposited from well-oxygenated and anoxic bottom waters.

In a strongly euxinic environment ($H_2S_{(aq)} \geq 11$ μM) in a restricted marine basin, soluble molybdate can be rapidly transformed to tetrathiomolybdate and quantitatively removed from bottom waters to sediments (Neubert et al., 2008). This scenario is represented by the modern Black Sea. Organic-rich sediments deposited from strongly euxinic waters in the Black Sea at water depths below 400 m yield δ^{98}Mo (2.0‰ to 2.4‰) similar to the open ocean (2.34 ± 0.10‰) even though the basin is strongly restricted (Barling et al., 2001; Arnold et al., 2004; Neubert et al., 2008). However, Mo isotope fractionation (0.5‰ ± 0.3‰) can occur between sediments and seawater under strongly euxinic conditions if there is incomplete removal of tetrathiomolybdate species from the overlying bottom waters (Nägler et al., 2011). In comparison, the δ^{98}Mo of organic-rich sediments (–0.5‰ to 2.2‰) deposited in weakly euxinic environments ($H_2S_{(aq)} < 11$ μM) displays a much larger range of Mo isotope fractionation (0.1‰ to 2.8‰), which may be caused by incomplete conversion of intermediate thiomolybdates to tetrathiomolybdate (Arnold et al., 2004; Siebert et al., 2006; Neubert et al., 2008; Dahl et al., 2010a; Nägler et al., 2011).

Hence, a general framework for δ^{98}Mo can be generated by combining all these observations. A more oxygenated ocean results in a heavy δ^{98}Mo for seawater, whereas

expanded ocean anoxia will lead to lighter δ^{98}Mo for seawater, which is especially true for the expansion of strongly euxinic conditions where the smallest extent of Mo isotope fractionation occurs. The δ^{98}Mo preserved in strongly euxinic ORMs has the greatest potential of all ORM to record the global seawater Mo isotope composition during deposition and thus capture direct information about global marine paleoredox conditions (e.g., Arnold et al., 2004; Dahl et al., 2010b; Kendall et al., 2011, 2015).

The euxinic Fjäcka Shale has an average δ^{98}Mo of 0.82 ± 0.26‰ (1SD), which is higher than the averages for the Kallholn Formation black shales (0.62 ± 0.16‰; 1SD) and gray shales (0.44 ± 0.06‰; 1SD) (Table 2). The most euxinic Fjäcka Shale from Stumsnäs #1 contains a higher average δ^{98}Mo (0.95 ± 0.27‰; 1SD) than that from Solberga #1 (0.66 ± 0.12‰; 1SD) (Table 2). Specifically, the highest Mo isotope composition of 1.28 ± 0.11‰ occurs in the Fjäcka Shale from Stumsnäs #1, which is associated with the highest Mo/TOC ratio (37.2 ppm/wt%). As lighter Mo isotopes are always preferentially removed into sediments, the highest Mo isotope composition in euxinic ORMs is most likely to mimic seawater δ^{98}Mo during deposition (e.g., Arnold et al., 2004; Dahl et al., 2010b). Because the Mo enrichments in the Fjäcka Shale are much higher, detrital Mo accounts for less than 5% of the total Mo budget of each sample, indicating that the authigenic Mo component dominates the δ^{98}Mo signature in these ORMs. Hence, the δ^{98}Mo of the Fjäcka Shale was not corrected for the presence of detrital Mo.

The heaviest δ^{98}Mo of the Fjäcka Shale may directly reflect coeval seawater δ^{98}Mo. If true, late Katian seawater had δ^{98}Mo similar to that of pre-Ediacaran Proterozoic seawater (1.0‰ to 1.4‰; Kendall et al., 2015 and references therein), which

indicates significant ocean anoxia already existed just prior to the end-Ordovician mass extinctions (ca. 447-443 Ma). However, such an interpretation is at odds with the relatively heavy U isotope compositions in the Fjäcka Shale, which suggest an appreciable extent of ocean oxygenation. Alternatively, the heaviest δ^{98}Mo recorded by the Fjäcka Shale is fractionated from the contemporaneous seawater Mo isotope composition.

The relatively low δ^{98}Mo (≤1.3‰) can be explained by either the operation of a Fe-Mn oxyhydroxide particulate shuttle that delivers isotopically light Mo to euxinic sediments (Algeo and Tribovillard, 2009; Herrmann et al., 2012) or the occurrence of Mo isotope fractionation between seawater and sediments under euxinic conditions (Arnold et al., 2004; Nägler et al., 2005, 2011; Neubert et al., 2008). It has been discussed previously that the particulate shuttle had a weak or negligible effect on the Mo isotope systematics of the Fjäcka Shale.

Hence, Mo isotope fractionation between seawater and authigenic solid Mo probably occurred under euxinic bottom water conditions. Only sediments with quantitative formation of tetrathiomolybdates and near-quantitative Mo removal from strongly euxinic bottom waters ($H_2S_{(aq)}$ > 11 μM) are associated with the smallest Mo isotope fractionation and thus capture the seawater δ^{98}Mo (e.g., deep Black Sea; Arnold et al., 2004; Neubert et al., 2008). Although high Mo enrichments and Fe speciation can fingerprint local euxinic bottom water conditions, they cannot further reveal whether the $H_2S_{(aq)}$ in the bottom water was high enough for quantitative formation of tetrathiomolybdates. In other words, these local redox proxies cannot distinguish between strongly euxinic and weakly euxinic environments. The modern Cariaco Basin and

shallower part (< 270 m) of the Black Sea contain weakly euxinic bottom waters ($H_2S_{(aq)}$ < 11 μM) but show different Mo isotope patterns. Specifically, δ^{98}Mo preserved in deep Cariaco Basin sediments and shallower sediments from the Black Sea varies from 1.5‰ to 2.2‰ (Arnold et al., 2004) and from –0.6‰ to 0.9‰ (Neubert et al., 2008), respectively. The Fjäcka Shale may be more similar to the deep Cariaco Basin instead of the shallow Black Sea when taking trace element abundances (e.g., Mo/TOC ratios) into consideration. Applying the observed Mo isotope fractionation of 0.1-0.8‰ in the deep Cariaco Basin to the heaviest δ^{98}Mo in the Fjäcka Shale suggests that the coeval late Katian seawater δ^{98}Mo is 1.4-2.1‰.

It is also possible that the Fjäcka Shale was deposited in a strongly euxinic setting but Mo removal from the bottom waters was not quantitative. This scenario is supported by the high Mo enrichments and Mo/TOC ratios in the Fjäcka Shale samples with the highest δ^{98}Mo (Fig. 4 and Fig. 6a) because only high dissolved Mo concentrations in bottom waters can result in such high Mo enrichments. A 0.5 ± 0.3‰ fractionation between strongly euxinic bottom waters and sediments may occur when there is quantitative conversion of all intermediate thiomolybdates to tetrathiomolybdates but incomplete removal of Mo from the bottom waters into sediments (Nägler et al., 2011). If this situation applies to the Fjäcka Shale, then the coeval seawater δ^{98}Mo should be around 1.5-2.1‰, which is similar with the estimate derived for the assumption of Cariaco-style weakly euxinic conditions.

In both cases (strongly and weakly euxinic conditions), the inferred late Katian ocean Mo isotope compositions (between 1.4‰ and 2.1‰) suggest an appreciable extent of ocean oxygenation. This interpretation is consistent with the heavy U isotope

compositions as well as the Mo/TOC ratios, which are significantly higher in the Fjäcka Shale (average = 13.5 ppm/wt%) compared with Proterozoic euxinic shales (average = 6.4 ppm/wt%; Scott et al., 2008). Such high Mo/TOC ratios point to a sizable global seawater Mo reservoir, which in turn requires an appreciable extent of ocean oxygenation (Scott et al., 2008).

5.4. Implications for late Ordovician ocean redox conditions

Molybdenum isotope fractionation between seawater and organic-rich sediments can still occur under weakly and strongly euxinic conditions when tetrathiomolybdate formation and removal to sediments is not quantitative. Any expression of Mo isotope fractionation results in preferential removal of lighter Mo isotopes to sediments. Hence, the heaviest Mo isotope composition from a stratigraphic interval is usually used to represent the most conservative estimate of contemporaneous seawater δ^{98}Mo for a specific time interval (Dahl et al., 2010b; Kendall et al., 2015). Dahl et al. (2010b) presented a compilation of Mo isotope data from ORMs through time, and Kendall et al. (2015) further updated this compilation by using only Mo isotope data from euxinic ORMs as well as re-normalizing all data to the newly established international Mo isotope standard NIST SRM 3134 (Goldberg et al., 2013; Nägler et al., 2014). Here, the Mo isotope compilation is updated by adding data from this study and two recently published papers (Fig. 9) (Chen et al., 2015; Zhou et al., 2015).

Figure 9

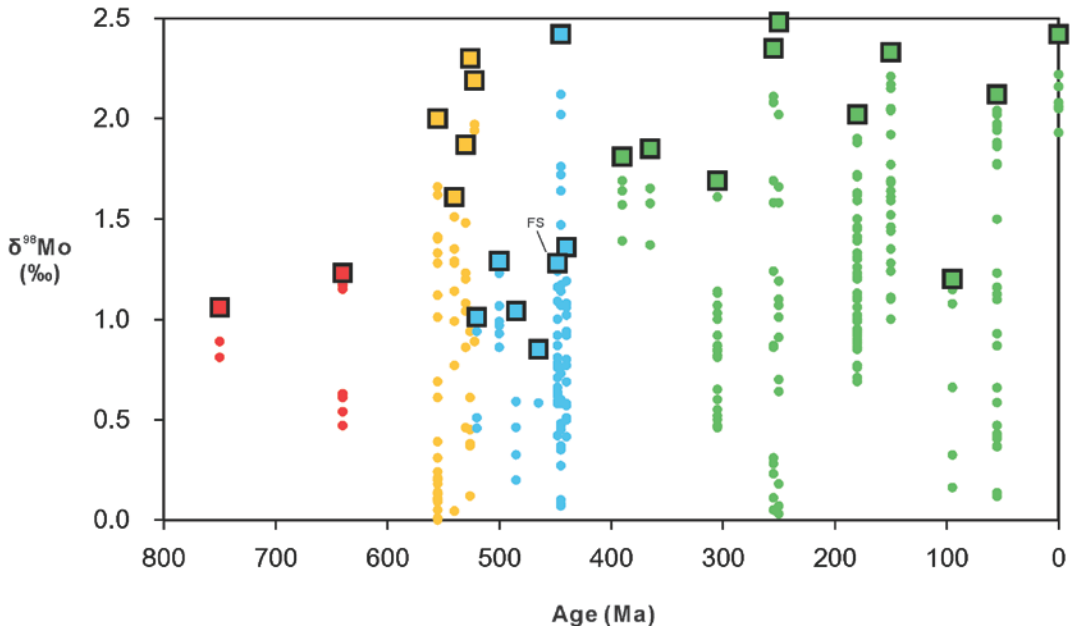

Fig. 9. Mo isotope compilation for euxinic ORM from the late Precambrian to present. FS represents the Fjäcka Shale analyzed in this study. Squares and circles represent the highest Mo isotope data and other Mo isotope data for each time period, respectively. Red = 750−640 Ma; yellow = 555−522 Ma; blue = 520−440 Ma; green = 390−0 Ma. Date sources: Kendall et al., 2015 and references therein; Chen et al., 2015; Zhou et al., 2015.

Although the low δ^{98}Mo in ORM deposited between 520 and 440 Ma is similar to that of ORM deposited before 640 Ma, it does not indicate a return to widely anoxic oceanic conditions in the early Paleozoic following instances of widespread ocean oxygenation in the late Ediacaran and early Cambrian. Temporal compilations of redox-sensitive Cr and U concentrations in ORMs through time yield a larger seawater Cr and U reservoir in the early Paleozoic than those of the Precambrian as a consequence of the Neoproterozoic oxygenation event (Reinhard et al., 2013; Partin et al., 2013b). Dahl et al. (2010b) suggested the low δ^{98}Mo still reflects a redox-stratified ocean, but with euxinic conditions in the middle water column along ocean margins and weakly oxygenated

waters in the deep ocean. The late Phanerozoic ocean is suggested to be extensively oxygenated, as revealed by high Mo isotope compositions in ORM from 390 Ma onwards (Dahl et al., 2010b), although short episodes of OAEs occurred episodically (Kendall et al., 2015 and references therein).

Comparing the Mo isotope compositions of the Fjäcka Shale with the rest of the early Paleozoic Mo isotope data is not easy because it is difficult to determine whether the early Paleozoic ORMs directly capture seawater δ^{98}Mo. Molybdenum isotope fractionations between seawater and sediments would have occurred if other early Paleozoic ORMs represent ancient analogues of the deep Cariaco Basin or shallow Black Sea (Arnold et al., 2004; Nägler et al., 2005; Neubert et al., 2008). To minimize the ambiguity posed by Mo isotope data in ORMs, we employed the novel U isotope system for inferring global ocean paleoredox conditions. In this study, the Fjäcka Shale Mo and U isotope data together point to a relatively well-oxygenated late Katian ocean although the extent of oxygenation was less than today. Subsequently, early Hirnantian ORM from South China capture a heaviest δ^{98}Mo signature that is similar to modern seawater δ^{98}Mo (Zhou et al., 2012, 2015), pointing to extensive ocean oxygenation in the framework of our interpretation. Lighter δ^{98}Mo signatures in most late Katian and Hirnantian ORM from South China may reflect local Mo isotope fractionation between seawater and sediments because of, for example, less intensely reducing conditions or non-quantitative removal of Mo from bottom waters in a fashion similar to the Fjäcka Shale. Low δ^{98}Mo (–0.3‰ to 0.6‰) in the late Katian Wufeng Formation ORMs from the Wangjiawan section in South China have Mo abundances of 12 to 51 ppm (n = 5) (Zhou et al., 2012, 2015). Samples with Mo concentrations lower than 25 ppm may indicate deposition from

non-euxinic bottom waters (Scott and Lyons, 2012). Sediments with Mo concentrations between 25 and 100 ppm can represent deposition under intermittently euxinic conditions (Scott and Lyons, 2012). Hence, the Wufeng Formation ORM may have been deposited under non-euxinic and intermittently weakly euxinic conditions, and thus may not capture the seawater δ^{98}Mo signature. Instead, large Mo isotope fractionations from seawater may be recorded by the Wufeng Formation, like those observed in the shallow Black Sea (Neubert et al., 2008).

Two samples from the early Hirnantian ORM in South China with the highest δ^{98}Mo (> 2‰) and the highest Mo abundances (> 100 ppm) are the most likely to represent deposition from locally strong euxinic bottom waters (Fig. 9) (Scott and Lyons, 2012). This combination of high Mo enrichment and high δ^{98}Mo is a robust signature of widespread ocean oxygenation (e.g., Dahl et al., 2010b; Kendall et al., 2015). Taken together with our inferred estimate of the late Katian seawater Mo isotope composition (1.4-2.1‰), we suggest that ocean oxygenation intensified from the late Katian to the early-mid Hirnantian.

Zhang et al. (2009) and Hammarlund et al. (2012) suggested that a positive excursion in $\delta^{34}S_{py}$ during the early-mid Hirnantian can be explained as an increase in pyrite burial, thus suggesting the possibility of expanded ocean anoxia as a mechanism for the first extinction pulse. On the contrary, Yan et al. (2009) and Zhang et al. (2011) attribute this observation to diagenetic effects. Hammarlund et al. (2012) further proposed that increased organic matter burial caused the positive HICE (e.g., Marshall and Middleton, 1990; Brenchley et al., 1994) and is associated with deep ocean anoxia. Melchin et al. (2013) argued that only when the stratigraphic trends in $\delta^{13}C$, $\delta^{34}S_{py}$, and

$\delta^{34}S_{sulfate}$ are strongly correlated can the hypothesis of expanded ocean anoxia be robust. Moreover, if increased burial of organic matter occurred and caused HICE, then TOC data should display a positive correlation with both $\delta^{13}C_{carb}$ and $\delta^{13}C_{org}$ (Gorjan et al., 2012). However, this pattern is not observed in currently available data, even in the deep sea sedimentary rocks of Chinese (Yan et al., 2009) and Arctic Canadian (Melchin and Holmden, 2006) sections. Hence, a sulfidic driver for the first extinction pulse during the early-mid Hirnantian (Hammarlund et al., 2012) is not fully supported by the data. On the contrary, our new U and Mo isotope data from the Fjäcka Shale together with Mo isotope data from Zhou et al. (2012, 2015) point to relatively well-oxygenated oceans during the late Katian followed by intensification of ocean oxygenation during the early-middle Hirnantian. Instead of interpreting HICE as a result of increased organic carbon burial, weathering of exposed carbonate platforms during eustatic sea-level fall triggered by the Hirnantian glaciation may be an alternative explanation (e.g., Kump et al. 1999; Melchin and Holmden, 2006).

Our hypothesis of relatively well-oxygenated late Katian oceans is also supported by data from other similarly-aged ORM in various depositional settings from the deep shelf to the base of the continental slope (Melchin et al., 2013). More than half of the localities documented were suggested to be deposited under oxic/suboxic conditions in the late Katian based on geochemical data ($\delta^{34}S$, trace element concentrations) and presence/absence of bioturbation (Melchin et al., 2013). Furthermore, ORM deposited from oxic/suboxic bottom waters are five times more abundant than ORM deposited from anoxic bottom waters in the mid-Hirnantian (Melchin et al., 2013). In contrast, more widespread black shale deposition occurred in the early Rhuddanian at the start of the

Silurian Period, suggesting an increase in global ocean anoxia at this time (Melchin et al., 2013).

In addition, low nitrogen isotope compositions (−1‰ to 1‰) from sediments deposited in the late Katian and at the Hirnantian-Rhuddanian boundary suggest that deep oceans during these times were relatively depleted of fixed nitrogen, resulting in a deficiency of nitrogen returning to the photic zone via oceanic upwelling to sustain algae productivity (LaPorte et al., 2009; Melchin et al., 2013). Hence, the low nitrogen isotope compositions indicate a somewhat greater extent of ocean anoxia compared with the modern ocean (Melchin et al., 2013), thus being consistent with our U and Mo isotope data from the euxinic Fjäcka Shale. During the Hirnantian glaciation, icehouse conditions will increase ocean ventilation, resulting in more downwelling of oxygenated surface waters, and therefore the reduction of oxygen-depleted deeper waters (LaPorte et al., 2009). Increased ocean oxygenation during the Hirnantian glaciation is consistent with the occurrence of modern seawater-like heavy Mo isotope compositions at this time in ORMs from South China (Zhou et al., 2012, 2015). Correspondingly, nitrogen isotope compositions during the early-mid Hirnantian do shift towards higher values (2‰ to 4‰), thus indicating less intense denitrification and a smaller extent of anoxia in the deep oceans (LaPorte et al., 2009; Melchin et al., 2013).

6. CONCLUSION

A combination of Mo, U, and Re enrichments, Mo/U and Mo/Re ratios, and Fe speciation clearly indicate three different bottom water redox conditions in the depositional environment for late Ordovician and early Silurian ORMs obtained from new drill cores in the Siljan ring district, central Sweden. Sedimentary Fe speciation and trace element records indicate an euxinic depositional environment for the Fjäcka Shale, fluctuations between euxinic and oxygenated conditions for black shales of the Kallholn Formation, and an oxygenated environment for gray shales equivalent to the upper Kallholn Formation.

New U and Mo isotope data from the euxinic Fjäcka Shale point to an appreciable extent of ocean oxygenation during the late Katian. The global ocean redox conditions at this time were intermediate between the modern oceans and some Phanerozoic oceanic anoxic events (e.g., OAE2, end-Permian). The high average authigenic $\delta^{238}U$ (−0.05‰ to 0.02‰) for the Fjäcka Shale (calculated assuming a range of detrital $\delta^{238}U$) suggests a seawater $\delta^{238}U$ of –0.5‰, which is only about 0.1‰ lower than modern seawater. Uranium isotope mass balance modeling reveals that the anoxic/euxinic sink comprised about 25% ± 25% of the U removal flux in the late Katian ocean, which is roughly two times larger than that of the present day (~10-15%). Although the highest $\delta^{98}Mo$ in the Fjäcka Shale is only about 1.3‰, we argue that Mo isotope fractionations between seawater and sediments likely occurred due to incomplete formation and/or removal of tetrathiomolybdate from bottom waters. At least incomplete removal of Mo from bottom waters is implied by the high Mo concentrations associated with the highest $\delta^{98}Mo$. Our

study thus shows the advantage of integrating U and Mo isotope data from ORMs to infer the extent of ancient global ocean oxygenation.

The heaviest δ^{98}Mo in the early Hirnantian (2.4‰) is similar to modern seawater (2.3‰) (Zhou et al., 2012, 2015), thus suggesting early Hirnantian ocean oxygenation was at a scale similar to that of the modern ocean. Hence, our data together with the previously published Mo isotope data for the Hirnantian indicates that ocean oxygenation intensified from the late Katian to the early-mid Hirnantian. This interpretation is supported by other geochemical evidence such as δ^{15}N trends across the Ordovician-Silurian transition (LaPorte et al., 2009; Melchin et al., 2013), suggesting that widespread ocean anoxia did not prevail throughout the Katian and Hirnantian (Zhang et al., 2009; Hammarlund et al., 2012).

REFERENCES

Ahmed, M., Lehnert, O., Fuentes, D. and Meinhold, G. (2014) Origin of oil and bitumen in the Late Devonian Siljan impact structure, central Sweden. *Organic Geochemistry, 68*, 13-26. doi: 10.1016/j.orggeochem.2013.12.010

Ainsaar, L., Kaljo, D., Martma, T., Meidla, T., Männik, P., Nõlvak, J. and Tinn, O. (2010) Middle and Upper Ordovician carbon isotope chemostratigraphy in Baltoscandia: A correlation standard and clues to environmental history. *Palaeogeography, Palaeoclimatology, Palaeoecology, 294*(3-4), 189-201. doi: 0.1016/j.palaeo.2010.01.003

Algeo, T. J. and Lyons, T. W. (2006) Mo-total organic carbon covariation in modern anoxic marine environments: Implications for analysis of paleoredox and paleohydrographic conditions. *Paleoceanography, 21*, PA1016. doi: 10.1029/2004pa001112

Algeo, T. J. and Maynard, J. B. (2004) Trace-element behavior and redox facies in core shales of Upper Pennsylvanian Kansas-type cyclothems. *Chemical Geology, 206*(3-4), 289-318. doi: 10.1016/j.chemgeo.2003.12.009

Algeo, T. J. and Tribovillard, N. (2009) Environmental analysis of paleoceanographic systems based on molybdenum–uranium covariation. *Chemical Geology, 268*(3-4), 211-225. doi: 10.1016/j.chemgeo.2009.09.001

Anbar, A. D., Duan, Y., Lyons, T. W., Arnold, G. L., Kendall, B., Creaser, R. A., Kaufman, A. J., Gordon, G. W., Scott, C., Garvin, J. and Buick, R. (2007) A

Whiff of Oxygen Before the Great Oxidation Event? *Science*, *317*(5846), 1903-1906. doi: 10.1126/science.1140325

Andersen, M. B., Romaniello, S., Vance, D., Little, S. H., Herdman, R. and Lyons, T. W. (2014) A modern framework for the interpretation of 238U/235U in studies of ancient ocean redox. *Earth and Planetary Science Letters*, *400*, 184-194. doi: 10.1016/j.epsl.2014.05.051

Andersen, M. B., Vance, D., Morford, J. L., Bura-Nakić, E., Breitenbach, S. F. M. and Och, L. (2016) Closing in on the marine 238U/235U budget. *Chemical Geology*, *420*, 11-22. doi: 10.1016/j.chemgeo.2015.10.041

Anderson, R. F. (1987) Redox behavior of uranium in an anoxic marine basin. *Uranium*, *3*(2-4), 145-164.

Anderson, R. F., Fleisher, M. Q. and Lehuray, A. P. (1989) Concentration, oxidation state, and particulate flux of uranium in the Black Sea. *Geochimica et Cosmochimica Acta*, *53*, 2215-2224.

Anderson, T. F. and Raiswell, R. (2004) Sources and mechanisms for the enrichment of highly reactive iron in euxinic Black Sea sediments. *American Journal of Science*, *304*, 203-233.

Archer, C. and Vance, D. (2008) The isotopic signature of the global riverine molybdenum flux and anoxia in the ancient oceans. *Nature Geoscience, 1*(9), 597-600. doi: 10.1038/ngeo282

Arnold, G. L., Anbar, A. D., Barling, J. and Lyons, T. W. (2004) Molybdenum isotope evidence for widespread anoxia in mid-Proterozoic oceans. *Science, 304*(5667), 87-90. doi: 10.1126/science.1091785

Asael, D., Tissot, F. L. H., Reinhard, C. T., Rouxel, O., Dauphas, N., Lyons, T. W., Ponzevera, E., Liorzou, C. and Chéron, S. (2013) Coupled molybdenum, iron and uranium stable isotopes as oceanic paleoredox proxies during the Paleoproterozoic Shunga Event. *Chemical Geology, 362*, 193-210. doi: 10.1016/j.chemgeo.2013.08.003

Barling, J., Arnold, G. L. and Anbar, A. D. (2001) Natural mass-dependent variations in the isotopic composition of molybdenum. *Earth and Planetary Science Letters, 193*, 447-457.

Barling, J. and Anbar, A. D. (2004) Molybdenum isotope fractionation during adsorption by manganese oxides. *Earth and Planetary Science Letters, 217*(3-4), 315-329. doi: 10.1016/s0012-821x(03)00608-3

Barnes, C. E. and Cochran, J. K. (1990) Uranium removal in oceanic sediments and the oceanic U balance. *Earth and Planetary Science Letters, 97*, 94-101.

Bauert, H., Isozaki, Y., Holmer, L. E., Aoki, K., Sakata, S. and Hirata, T. (2014) New U–Pb zircon ages of the Sandbian (Upper Ordovician) “Big K-bentonite” in Baltoscandia (Estonia and Sweden) by LA-ICPMS. *Gff, 136*(1), 30-33. doi: 10.1080/11035897.2013.862854

Bergström, S. M., Chen, X. U., Gutiérrez-Marco, J. C. and Dronov, A. (2009) The new chronostratigraphic classification of the Ordovician System and its relations to major regional series and stages and to $\delta^{13}C$ chemostratigraphy. *Lethaia, 42*(1), 97-107. doi: 10.1111/j.1502-3931.2008.00136.x

Bergström, S. M., Huff, W. D., Saltzman, M. R., Kolata, D. R. and Leslie, S. A. (2004) The greatest volcanic ash falls in the Phanerozoic: Trans-Atlantic relations of the

Ordovician Millbrig and Kinnekulle K-Bentonites. *The Sedimentary Record, 2*(4), 4-8.

Bergström, S. M., Saltzman, M. M. and Schmitz, B. (2006) First record of the Hirnantian (Upper Ordovician) δ13C excursion in the North American Midcontinent and its regional implications. *Geological Magazine, 143*(05), 657-678. doi: 10.1017/s0016756806002469

Bergström, S. M., Toprak, F. Ö., Huff, W. D. and Mundil, R. (2008) Implications of a new, biostratigraphically well-controlled, radio-isotopic age for the lower Telychian Stage of the Llandovery Series (Lower Silurian, Sweden). *Episodes, 31*, 309-314.

Bergström, S. M., Young, S. and Schmitz, B. (2010) Katian (Upper Ordovician) $\delta^{13}C$ chemostratigraphy and sequence stratigraphy in the United States and Baltoscandia: A regional comparison. *Palaeogeography, Palaeoclimatology, Palaeoecology, 296*(3-4), 217-234. doi: 10.1016/j.palaeo.2010.02.035

Biegeleisen, J. (1996) Nuclear Size and Shape Effects in Chemical Reactions. Isotope Chemistry of the Heavy Elements. *Journal of the American Chemical Society, 118,* 3676-3680.

Brennecka, G. A., Herrmann, A. D., Algeo, T. J. and Anbar, A. D. (2011a) Rapid expansion of oceanic anoxia immediately before the end-Permian mass extinction. *Proceedings of the National Academy of Sciences, 108*, 17631-17634. doi: 10.1073/pnas.1106039108/-/DCSupplemental

Brennecka, G. A., Wasylenki, L. E., Bargar, J. R., Weyer, S. and Anbar, A. D. (2011b) Uranium isotope fractionation during adsorption to Mn-oxyhydroxides.

Environmental Science and Technology, *45*(4), 1370-1375. doi: 10.1021/es103061v

Brenchley, P.J., 1989, The Late Ordovician extinction, *in* Donovan, S.K., ed., Mass Extinctions: Processes and Evidence: London, Belhaven Press, p. 104–132.

Brenchley, P. J., Carden, G. A., Hints, L., Kaljo, D., Marshall, J. D., Martma, T., Meidla, T. and Nõlvak, J. (2003) High-resolution stable isotope stratigraphy of Upper Ordovician sequences: Constraints on the timing of bioevents and environmental changes associated with mass extinction and glaciation. *Geological Society of America Bulletin, 115*, 89-104.

Brenchley, P. J., Marshall, J. D., Carden, G. A. F., Robertson, D. B. R., Long, D. G. F., Meidla, T., Hints, L. and Anderson, T. F. (1994) Bathymetric and isotopic evidence for a short-lived Late Ordovician glaciation in a greenhouse period. *Geology*, *22*, 295-298.

Brenchley, P. J., Marshall, J. D. and Underwood, C. J. (2001) Do all mass extinctions represent an ecological crisis? Evidence from the Late Ordovician. *Geological Journal, 36*, 329-340.

Brennecka, G. A., Wasylenki, L. E., Bargar, J. R., Weyer, S. and Anbar, A. D. (2011a) Uranium isotope fractionation during adsorption to Mn-oxyhydroxides. *Environmental Science and Technology*, *45*(4), 1370-1375. doi: 10.1021/es103061v

Brennecka, G. A., Herrmann, A. D., Algeo, T. J., & Anbar, A. D. (2011b). Rapid expansion of oceanic anoxia immediately before the end-Permian mass extinction.

Proceedings of the National Academy of Sciences, 108, 17631-17634. doi: 10.1073/pnas.1106039108/-/DCSupplemental

Canfield, D. E., Poulton, S. W. and Narbonne, G. M. (2007) Late-Neoproterozoic deep-ocean oxygenation and the rise of animal life. *Science, 315*(5808), 92-95. doi: 10.1126/science.1135013

Canfield, D. E., Raiswell, R., Westrich, J. T., Reaves, C. M. and Berner, R. A. (1986) The use of chromium reduction in the analysis of reduced inorganic sulfur in sediments and shales. *Chemical Geology, 54*, 149-155.

Cederbom, C., Larson, S. A., Tullborg, E. and Stiberg, J. (2000) Fission track thermochronology applied to Phanerozoic thermotectonic events in central and southern Sweden. *Tectonophysics, 316*, 153-167.

Chappaz, A., Lyons, T. W., Gregory, D. D., Reinhard, C. T., Gill, B. C., Li, C. and Large, R. R. (2014) Does pyrite act as an important host for molybdenum in modern and ancient euxinic sediments? *Geochimica et Cosmochimica Acta, 126*, 112-122. doi: 10.1016/j.gca.2013.10.028

Chen, X., Ling, H. F., Vance, D., Shields-Zhou, G. A., Zhu, M., Poulton, S. W., Och, L. M., Jiang, S. Y., Li, D., Cremonese, L. and Archer, C. (2015) Rise to modern levels of ocean oxygenation coincided with the Cambrian radiation of animals. *Nature Communications, 6*, 7142. doi: 10.1038/ncomms8142

Cherns, L. and Wheeley, J. R. (2007) A pre-Hirnantian (Late Ordovician) interval of global cooling – The Boda event re-assessed. *Palaeogeography, Palaeoclimatology, Palaeoecology, 251*(3-4), 449-460. doi: 10.1016/j.palaeo.2007.04.010

Christidis, G. E. and Huff, W. D. (2009) Geological Aspects and Genesis of Bentonites. *Elements, 5*(2), 93-98. doi: 10.2113/gselements.5.2.93

Cocks, L. R. M. and Torsvik, T. H. (2002) Earth geography from 500 to 400 million years ago: a faunal and palaeomagnetic review. *Journal of the Geological Society, London, 159*, 631-644.

Cocks, L. R. M. and Torsvik, T. H. (2005) Baltica from the late Precambrian to mid-Palaeozoic times: The gain and loss of a terrane's identity. *Earth-Science Reviews, 72*(1-2), 39-66. doi: 10.1016/j.earscirev.2005.04.001

Cohen, K. M., Finney, S. C., Gibbard, P. L. and Fan, J. (2013) The ICS International Chronostratigraphic Chart. *Episodes, 36*(3), 199-204.

Collier, R. W. (1985) Molybdenum in the Northeast Pacific Ocean. *Limnology and Oceanography, 30*(6), 1352-1354.

Cramer, B. D., Brett, C. E., Melchin, M. J., Männik, P., Kleffner, M. A., McLaughlin, P. I., Loydell, D. K., Munnecke, A., Jeppsson, L., Corradini, C., Brunton, F. R. and Saltzman, M. R. (2011) Revised correlation of Silurian Provincial Series of North America with global and regional chronostratigraphic units and $\delta 13C_{carb}$ chemostratigraphy. *Lethaia, 44*(2), 185-202. doi: 10.1111/j.1502-3931.2010.00234.x

Crusius, J., Calvert, S., Pedersen, T. and Sage, D. (1996) Rhenium and molybdenum enrichments in sediments as indicators of oxic, suboxic and sulfidic conditions of deposition. *Earth and Planetary Science Letters, 145*, 65-78.

Dahl, T. W., Anbar, A. D., Gordon, G. W., Rosing, M. T., Frei, R. and Canfield, D. E. (2010a) The behavior of molybdenum and its isotopes across the chemocline and

in the sediments of sulfidic Lake Cadagno, Switzerland. *Geochimica et Cosmochimica Acta, 74*(1), 144-163. doi: 10.1016/j.gca.2009.09.018

Dahl, T. W., Hammarlund, E. U., Anbar, A. D., Bond, D. P. G., Gill, B. C., Gordon, G. W., Knoll, A. H., Nielsen, A. T., Schovsbo, N. H. and Canfield, D. E. (2010b) Devonian rise in atmospheric oxygen correlated to the radiations of terrestrial plants and large predatory fish. *Proceedings of the National Academy of Sciences, 107*(42), 17911-17915. doi: 10.1073/pnas.1011287107/-/DCSupplemental

Dahl, T. W., Boyle, R. A., Canfield, D. E., Connelly, J. N., Gill, B. C., Lenton, T. M. and Bizzarro, M. (2014) Uranium isotopes distinguish two geochemically distinct stages during the later Cambrian SPICE event. *Earth and Planetary Science Letters, 401*, 313-326. doi: 10.1016/j.epsl.2014.05.043

Dahl, T. W., Canfield, D. E., Rosing, M. T., Frei, R. E., Gordon, G. W., Knoll, A. H. and Anbar, A. D. (2011) Molybdenum evidence for expansive sulfidic water masses in ~750Ma oceans. *Earth and Planetary Science Letters, 311*(3-4), 264-274. doi: 10.1016/j.epsl.2011.09.016

Dahl, T. W., Chappaz, A., Fitts, J. P. and Lyons, T. W. (2013) Molybdenum reduction in a sulfidic lake: Evidence from X-ray absorption fine-structure spectroscopy and implications for the Mo paleoproxy. *Geochimica et Cosmochimica Acta, 103*, 213-231. doi: 10.1016/j.gca.2012.10.058

Delabroye, A., and Vecoli, M. (2010) The end-Ordovician glaciation and the Hirnantian Stage: A global review and questions about Late Ordovician event stratigraphy. *Earth-Science Reviews, 98*(3-4), 269-282. doi: 10.1016/j.earscirev.2009.10.010

Duan, Y., Anbar, A. D., Arnold, G. L., Lyons, T. W., Gordon, G. W. and Kendall, B. (2010. Molybdenum isotope evidence for mild environmental oxygenation before the Great Oxidation Event. *Geochimica et Cosmochimica Acta, 74*(23), 6655-6668. doi: 10.1016/j.gca.2010.08.035

Dunk, R. M., Mills, R. A. and Jenkins, W. J. (2002) A reevaluation of the oceanic uranium budget for the Holocene. *Chemical Geology, 190,* 45-67.

Ebbestad, J. O. R. and Högström, A. E. S. (2007) Ordovician of the Siljan district, Sweden. In: Ebbestad, J. O. R., Wickström, L. M., Högström, A. E. S. (Eds.) WOGOGOB 2007. 9th Meeting of the Working Group on Ordovician Geology of Baltoscandia. Field guide and Abstracts. *Sveriges Geologiska Undersökning Rapporter och meddelanden, 128,* 7-26.

Ebbestad, J. O. R., Högström, A. E. S., Frisk, Å. M., Martma, T., Kaljo, D., Kröger, B. and Pärnaste, H. (2014) Terminal Ordovician stratigraphy of the Siljan district, Sweden. *Gff,* 1-21. doi: 10.1080/11035897.2014.945620

Emerson, S. R. and Huested, S. S. (1991) Ocean anoxia and the concentrations of molybdenum and vanadium in seawater. *Marine Chemistry, 34,* 177-196.

Erickson, B. E. and Helz, G. R. (2000) Molybdenum(VI) speciation in sulfidic waters: Stability and lability of thiomolybdates. *Geochimica et Cosmochimica Acta, 64*(7), 1149-1158.

Finlay, A. J., Selby, D. and Gröcke, D. R. (2010) Tracking the Hirnantian glaciation using Os isotopes. *Earth and Planetary Science Letters, 293*(3-4), 339-348. doi: 10.1016/j.epsl.2010.02.049

Finnegan, S., Bergmann, K., Eiler, J. M., Jones, D. S., Fike, D. A., Eisenman, I., Hughes, N. C., Tripati, A. K. and Fischer, W. W. (2011) The Magnitude and Duration of Late Ordovician - Early Silurian Glaciation. *Science, 331*, 903-906.

Finney, S. C., Berry, W. B. N., Cooper, J. D., Ripperdan, R. L., Sweet, W. C., Jacobson, S. R., Soufiane, A., Achab, A. and Noble, P. J. (1999) Late Ordovician mass extinction: A new perspective from stratigraphic sections in central Nevada. *Geology, 27*, 215-218.

Fortey, R. A. and Cocks, L. R. M. (2005) Late Ordovician global warming—The Boda event. *Geology*, *33*(5), 405-408. doi: 10.1130/g21180.1

Gee, D. G., Juhlin, C., Pascal, C. and Robinson, P. (2010) Collisional Orogeny in the Scandinavian Caledonides (COSC). *Gff*, *132*(1), 29-44. doi: 10.1080/11035891003759188

Grieve, R. A. F. (1988) The formation of large impact structures and constraints on the nature of Siljan. In A. Boden & K. G. Eriksson (eds.): Deep drilling in crystalline bedrock, 328-348. Vol. 1. The deep gas drilling in the Siljan impact structure, Sweden and Astroblemes Proceeding of the International Symposium. Springer Verlag, Berlin

Gold, T. and Soter, S. (1980) The deep-earth gas hypothesis. *Scientific American, 242*, 154-161.

Goldberg, T., Gordon, G., Izon, G., Archer, C., Pearce, C. R., McManus, J., Anbar, A. D. and Rehkämper, M. (2013) Resolution of inter-laboratory discrepancies in Mo isotope data: an intercalibration. *Journal of Analytical Atomic Spectrometry, 28*(5), 724. doi: 10.1039/c3ja30375f

Gordon, G. W., Lyons, T. W., Arnold, G. L., Roe, J., Sageman, B. B. and Anbar, A. D. (2009) When do black shales tell molybdenum isotope tales? *Geology, 37*(6), 535-538. doi: 10.1130/g25186a.1

Gorjan, P., Kaiho, K., Fike, D. A. and Xu, C. (2012) Carbon- and sulfur-isotope geochemistry of the Hirnantian (Late Ordovician) Wangjiawan (Riverside) section, South China: Global correlation and environmental event interpretation. *Palaeogeography, Palaeoclimatology, Palaeoecology, 337-338*, 14-22. doi: 10.1016/j.palaeo.2012.03.021

Goto, K. T., Anbar, A. D., Gordon, G. W., Romaniello, S. J., Shimoda, G., Takaya, Y., Tokumaru, A., Nozaki, T., Suzuki, K., Machida, S., Hanyu, T. and Usui, A. (2014) Uranium isotope systematics of ferromanganese crusts in the Pacific Ocean: Implications for the marine 238U/235U isotope system. *Geochimica et Cosmochimica Acta, 146*, 43-58. doi: 10.1016/j.gca.2014.10.003

Grahn, Y. (1998) Lower Silurian (Llandovery-Middle Wenlock) Chitinozoa and biostratigraphy of the mainland of Sweden. *Gff, 120*(3), 273-283. doi: 10.1080/11035899809453218

Hammarlund, E. U., Dahl, T. W., Harper, D. A. T., Bond, D. P. G., Nielsen, A. T., Bjerrum, C. J., Schovsbo, N. H., Schönlaub, H. P., Zalasiewicz, J. A. and Canfield, D. E. (2012) A sulfidic driver for the end-Ordovician mass extinction. *Earth and Planetary Science Letters, 331-332*, 128-139. doi: 10.1016/j.epsl.2012.02.024

Haq, B. U. and Schutter, S. R. (2008) A Chronology of Paleozoic Sea-Level Changes. *Science, 322*, 64-68.

Helz, G. R., Bura-Nakić, E., Mikac, N. and Ciglenečki, I. (2011) New model for molybdenum behavior in euxinic waters. *Chemical Geology, 284*(3-4), 323-332. doi: 10.1016/j.chemgeo.2011.03.012

Helz, G. R., Miller, C. V., Charnock, J. M., Mosselmans, J. F. W., Pattrick, R. A. D., Garner, C. D. and Vaughan, D. J. (1996) Mechanism of molybdenum removal from the sea and its concentration in black shales: EXAFS evidence. *Geochimica et Cosmochimica Acta, 60*(19), 3631-3642.

Herrmann, A. D., Kendall, B., Algeo, T. J., Gordon, G. W., Wasylenki, L. E. and Anbar, A. D. (2012) Anomalous molybdenum isotope trends in Upper Pennsylvanian euxinic facies: Significance for use of δ98Mo as a global marine redox proxy. *Chemical Geology, 324-325*, 87-98. doi: 10.1016/j.chemgeo.2012.05.013

Högström, A. E. S., Sturkell, E., Ebbestad, J. O. R., Lindström, M. and Ormö, J. (2010) Concentric impact structures in the Palaeozoic of Sweden – the Lockne and Siljan craters. *Gff, 132*(1), 65-70. doi: 10.1080/11035890903469971

Holm, S., Alwmark, C., Alvarez, W. and Schmitz, B. (2011) Shock barometry of the Siljan impact structure, Sweden. *Meteoritics and Planetary Science, 46*(12), 1888-1909. doi: 10.1111/j.1945-5100.2011.01303.x

Holmden, C., Amini, M. and Francois, R. (2015) Uranium isotope fractionation in Saanich Inlet: A modern analog study of a paleoredox tracer. *Geochimica et Cosmochimica Acta, 153*, 202-215. doi: 10.1016/j.gca.2014.11.012

Huff, W. D., Kolata, D. R., Bergström, S. M. and Zhang, Y. (1996) Large-magnitude Middle Ordovician volcanic ash falls in North America and Europe: dimensions,

emplacement and post-emplacement characteristics. *Journal of Volcanology and Geothermal Research, 73,* 285-301.

Huigen, Y. and Andriessen, P. (2004) Thermal effects of Caledonian foreland basin formation, based on fission track analyses applied on basement rocks in central Sweden. *Physics and Chemistry of the Earth, Parts A/B/C, 29*(10), 683-694. doi: 10.1016/j.pce.2004.03.006

Jourdan, F., Reimold, W. U. and Deutsch, A. (2012) Dating Terrestrial Impact Structures. *Elements, 8*(1), 49-53. doi: 10.2113/gselements.8.1.49

Juhlin, C. (1990) Interpretation of the reflections in the Siljan Ring area based on results from the Gravberg-1 borehole. *Tectonophysics, 173,* 345-360.

Kendall, B., Brennecka, G. A., Weyer, S. and Anbar, A. D. (2013) Uranium isotope fractionation suggests oxidative uranium mobilization at 2.50Ga. *Chemical Geology, 362,* 105-114. doi: 10.1016/j.chemgeo.2013.08.010

Kendall, B., Creaser, R. A., Gordon, G. W. and Anbar, A. D. (2009) Re–Os and Mo isotope systematics of black shales from the Middle Proterozoic Velkerri and Wollogorang Formations, McArthur Basin, northern Australia. *Geochimica et Cosmochimica Acta, 73*(9), 2534-2558. doi: 10.1016/j.gca.2009.02.013

Kendall, B., Gordon, G. W., Poulton, S. W. and Anbar, A. D. (2011) Molybdenum isotope constraints on the extent of late Paleoproterozoic ocean euxinia. *Earth and Planetary Science Letters, 307*(3-4), 450-460. doi: 10.1016/j.epsl.2011.05.019

Kendall, B., Komiya, T., Lyons, T. W., Bates, S. M., Gordon, G. W., Romaniello, S. J., Jiang, G., Creaser, R. A., Xiao, S., McFadden, K., Sawaki, Y., Tahata, M., Shu, D., Han, J., Li, Y., Chu, X. and Anbar, A. D. (2015) Uranium and molybdenum

isotope evidence for an episode of widespread ocean oxygenation during the late Ediacaran Period. *Geochimica et Cosmochimica Acta, 156*, 173-193. doi: 10.1016/j.gca.2015.02.025

Komor, S. C., Valley, J. W. and Brown, P. E. (1988) Fluid-inclusion evidence for impact heating at the Siljan Ring, Sweden. *Geology, 16*, 711-715.

Ku, T. L., Knauss, K. G. and Mathieu, G. G. (1977) Uranium in open ocean: concentration and isotopic composition*. *Deep Sea Research, 24*, 1005-1017.

Kump, L. R., Arthur, M. A., Patzkowsky, M. E., Gibbs, M. T., Pinkus, D. S. and Sheehan, P. M. (1999) A weathering hypothesis for glaciation at high atmospheric pCO2 during the Late Ordovician. *Palaeogeography, Palaeoclimatology, Palaeoecology, 152*, 173-187.

Langmuir, D. (1978) Uranium solution-mineral equilibria at low temperatures with applications to sedimentary ore deposits. *Geochimica et Cosmochimica Acta, 42*, 547-569.

LaPorte, D. F., Holmden, C., Patterson, W. P., Loxton, J. D., Melchin, M. J., Mitchell, C. E., Finney, S. C. and Sheets, H. D. (2009) Local and global perspectives on carbon and nitrogen cycling during the Hirnantian glaciation. *Palaeogeography, Palaeoclimatology, Palaeoecology, 276*(1-4), 182-195. doi: 10.1016/j.palaeo.2009.03.009

Larson, S. A., Tullborg, E., Cederbom, C. and Stiberg, J. (1999) Sveconorwegian and Caledonian foreland basins in the Baltic Shield revealed by fission-track thermochronology. *Terra Nova, 11*, 210-215.

Lehnert, O., Meinhold, G., Arslan, A., Ebbestad, J. O. R. and Calner, M. (2013) Ordovician stratigraphy of the Stumsnäs 1 drill core from the southern part of the Siljan Ring, central Sweden. *Gff, 135*(2), 204-212. doi: 10.1080/11035897.2013.813582

Lehnert, O., Meinhold, G., Bergström, S. M., Calner, M., Ebbestad, J. O. R., Egenhoff, S., Frisk, Å. M., Hannah, J. L., Högström, A. E. S., Huff, W. D., Juhlin, C., Maletz, J., Stein, H. J., Sturkell, E. and Vandenbroucke, T. R. A. (2012) New Ordovician–Silurian drill cores from the Siljan impact structure in central Sweden: an integral part of the Swedish Deep Drilling Program. *Gff, 134*(2), 87-98. doi: 10.1080/11035897.2012.692707

Li, C., Love, G. D., Lyons, T. W., Fike, D. A., Sessions, A. L. and Chu, X. (2010) A stratified redox model for the Ediacaran ocean. *Science, 328*(5974), 80-83. doi: 10.1126/science.1182369

Lorenz, H. (2010) The Swedish Deep Drilling Program: For Science and Society. *Gff, 132*(1), 25-27. doi: 10.1080/11035891003763354

Lyons, T. W. and Severmann, S. (2006) A critical look at iron paleoredox proxies: New insights from modern euxinic marine basins. *Geochimica et Cosmochimica Acta, 70*(23), 5698-5722. doi: 10.1016/j.gca.2006.08.021

Marshall, J. D. and Middleton, P. D. (1990) Changes in marine isotopic composition and the late Ordovician glaciation. *Journal of the Geological Society, London, 147*, 1-4.

März, C., Poulton, S. W., Beckmann, B., Küster, K., Wagner, T. and Kasten, S. (2008) Redox sensitivity of P cycling during marine black shale formation: Dynamics of

sulfidic and anoxic, non-sulfidic bottom waters. *Geochimica et Cosmochimica Acta, 72*(15), 3703-3717. doi: 10.1016/j.gca.2008.04.025

McLennan, S. M. (2001) Relationships between the trace element composition of sedimentary rocks and upper continental crust. *Geochemistry, Geophysics, Geosystems, 2*, Paper number 2000GC000109.

McManus, J., Berelson, W. M., Severmann, S., Poulson, R. L., Hammond, D. E., Klinkhammer, G. P. and Holm, C. (2006) Molybdenum and uranium geochemistry in continental margin sediments: Paleoproxy potential. *Geochimica et Cosmochimica Acta, 70*(18), 4643-4662. doi: 10.1016/j.gca.2006.06.1564

McManus, J., Nägler, T. F., Siebert, C., Wheat, C. G. and Hammond, D. E. (2002) Oceanic molybdenum isotope fractionation: Diagenesis and hydrothermal ridge-flank alteration. *Geochemistry, Geophysics, Geosystems, 3*(12). doi: 10.1029/2002GC000356

Melchin, M. J. and Holmden, C. (2006) Carbon isotope chemostratigraphy in Arctic Canada: Sea-level forcing of carbonate platform weathering and implications for Hirnantian global correlation. *Palaeogeography, Palaeoclimatology, Palaeoecology, 234*(2-4), 186-200. doi: 10.1016/j.palaeo.2005.10.009

Melchin, M. J., Mitchell, C. E., Holmden, C. and Storch, P. (2013) Environmental changes in the Late Ordovician-early Silurian: Review and new insights from black shales and nitrogen isotopes. *Geological Society of America Bulletin, 125*(11-12), 1635-1670. doi: 10.1130/b30812.1

Miller, C. A., Peucker-Ehrenbrink, B., Walker, B. D. and Marcantonio, F. (2011) Re-assessing the surface cycling of molybdenum and rhenium. *Geochimica et Cosmochimica Acta, 75*(22), 7146-7179. doi: 10.1016/j.gca.2011.09.005

Montoya-Pino, C., Weyer, S., Anbar, A. D., Pross, J., Oschmann, W., van de Schootbrugge, B. and Arz, H. W. (2010) Global enhancement of ocean anoxia during Oceanic Anoxic Event 2: A quantitative approach using U isotopes. *Geology, 38*(4), 315-318. doi: 10.1130/g30652.1

Morford, J. L. and Emerson, S. (1999) The geochemistry of redox sensitive trace metals in sediments. *Geochimica et Cosmochimica Acta*, *63*(11/12), 1735-1750.

Morford, J. L., Emerson, S. R., Breckel, E. J. and Kim, S. H. (2005) Diagenesis of oxyanions (V, U, Re, and Mo) in pore waters and sediments from a continental margin. *Geochimica et Cosmochimica Acta, 69*(21), 5021-5032. doi: 10.1016/j.gca.2005.05.015

Nägler, T. F., Siebert, C., Lüschen, H. and Böttcher, M. E. (2005) Sedimentary Mo isotope record across the Holocene fresh–brackish water transition of the Black Sea. *Chemical Geology, 219*(1-4), 283-295. doi: 10.1016/j.chemgeo.2005.03.006

Nägler, T. F., Neubert, N., Böttcher, M. E., Dellwig, O. and Schnetger, B. (2011) Molybdenum isotope fractionation in pelagic euxinia: Evidence from the modern Black and Baltic Seas. *Chemical Geology, 289*(1-2), 1-11. doi: 10.1016/j.chemgeo.2011.07.001

Nägler, T. F., Anbar, A. D., Archer, C., Goldberg, T., Gordon, G. W., Greber, N. D., Siebert, C., Sohrin, Y. and Vance, D. (2014) Proposal for an International Molybdenum Isotope Measurement Standard and Data Representation.

Geostandards and Geoanalytical Research, *38*(2), 149-151. doi: 10.1111/j.1751-908X.2013.00275.x

Nakagawa, Y., Takano, S., Firdaus, M. L., Norsuye, K., Hirata, T., Vance, D. and Sohrin, Y. (2012) The molybdenum isotopic composition of the modern ocean. *Geochimica et Cosmochimica Acta, 46*, 131-141.

Neubert, N., Nägler, T. F. and Böttcher, M. E. (2008) Sulfidity controls molybdenum isotope fractionation into euxinic sediments: Evidence from the modern Black Sea. *Geology, 36*(10), 775-778. doi: 10.1130/g24959a.1

Noordmann, J., Weyer, S., Montoya-Pino, C., Dellwig, O., Neubert, N., Eckert, S., Paetzel, M. and Böttcher, M. E. (2015) Uranium and molybdenum isotope systematics in modern euxinic basins: Case studies from the central Baltic Sea and the Kyllaren fjord (Norway). *Chemical Geology, 396*, 182-195. doi: 10.1016/j.chemgeo.2014.12.012

Noordmann, J., Weyer, S., Sharma, M., Georg, R., Rausch, S. and Bach, W. (2010) Fractionation of 238U/235U in rivers and hydrothermal systems: Constraints for the oceanic U isotope cycle. *American Geophysical Union, Fall Meeting*, Abstract #V31B-2330.

Noordmann, J., Weyer, S., Sharma, M., Georg, R. B., Rausch, S. and Bach, W. (2011) Fractionation of 238U/235U during weathering and hydrothermal alteration. *Mineralogical Magazine,* A1548.

Nõlvak, J., Hints, O. and Männik, P. (2006) Ordovician timescale in Estonia: recent developments. *Proceedings of the Estonian Academy of Sciences, Geology, 55*, 95-108.

Papasikas, N. and Juhlin, C. (1997) Interpretation of reflections from the central part of the Siljan Ring impact structure based on results from the Stenberg-1 borehole. *Tectonophysics, 269,* 237-245.

Partin, C. A., Lalonde, S. V., Planavsky, N. J., Bekker, A., Rouxel, O. J., Lyons, T. W. and Konhauser, K. O. (2013a) Uranium in iron formations and the rise of atmospheric oxygen. *Chemical Geology, 362*, 82-90. doi: 10.1016/j.chemgeo.2013.09.005

Partin, C. A., Bekker, A., Planavsky, N. J., Scott, C. T., Gill, B. C., Li, C., Podkovyrov, V., Maslov, A., Konhauser, K. O., Lalonde, S. V., Love, G. D., Poulton, S. W. and Lyons, T. W. (2013b) Large-scale fluctuations in Precambrian atmospheric and oceanic oxygen levels from the record of U in shales. *Earth and Planetary Science Letters, 369-370,* 284-293. doi: 10.1016/j.epsl.2013.03.031

Pearce, C. R., Burton, K. W., von Strandmann, P. A. E. P., James, R. H. and Gíslason, S. R. (2010) Molybdenum isotope behaviour accompanying weathering and riverine transport in a basaltic terrain. *Earth and Planetary Science Letters, 295*(1-2), 104-114. doi: 10.1016/j.epsl.2010.03.032

Poulson, R. L., Siebert, C., McManus, J. and Berelson, W. M. (2006) Authigenic molybdenum isotope signatures in marine sediments. *Geology, 34*(8), 617. doi: 10.1130/g22485.1

Poulson Brucker, R. L., McManus, J., Severmann, S. and Berelson, W. M. (2009) Molybdenum behavior during early diagenesis. *Geochemistry, Geophysics, Geosystems, 10*(6), Q06010. doi: 10.1029/2008GC002180

Poulton, S. W. and Canfield, D. E. (2005) Development of a sequential extraction procedure for iron: implications for iron partitioning in continentally derived particulates. *Chemical Geology, 214*(3-4), 209-221. doi: 10.1016/j.chemgeo.2004.09.003

Poulton, S. W. and Canfield, D. E. (2011) Ferruginous Conditions: A Dominant Feature of the Ocean through Earth's History. *Elements, 7*(2), 107-112. doi: 10.2113/gselements.7.2.107

Poulton, S. W., Fralick, P. W. and Canfield, D. E. (2004) The transition to a sulphidic ocean ~1.84 billion years ago. *Nature, 431*, 173-177. doi: 10.1038/nature02863

Poulton, S. W., Fralick, P. W. and Canfield, D. E. (2010) Spatial variability in oceanic redox structure 1.8 billion years ago. *Nature Geoscience, 3*, 486-490. doi: 10.1038/ngeo889

Poulton, S. W. and Raiswell, R. (2002) The low-temperature geochemical cycle of iron: From continental fluxes to marine sediment deposition. *American Journal of Science, 302*, 774-805.

Raiswell, R. and Canfield, D. E. (1998) Sources of iron for pyrite formation in marine sediments. *American Journal of Science, 298*, 219-245.

Reimold, W. U., Kelley, S. P., Sherlock, S. C., Henkel, H. and Koeberl, C. (2005) Laser argon dating of melt breccias from the Siljan impact structure, Sweden: Implications for a possible relationship to Late Devonian extinction events. *Meteoritics and Planetary Science, 40*(4), 591-607.

Reinhard, C. T., Planavsky, N. J., Robbins, L. J., Partin, C. A., Gill, B. C., Lalonde, S. V., Bekker, A., Konhauser, K. O. and Lyons, T. W. (2013) Proterozoic ocean redox

and biogeochemical stasis. *Proceedings of the National Academy of Sciences, 110*(14), 5357-5362. doi: 10.1073/pnas.1208622110

Reinhard, C. T., Raiswell, R., Scott, C., Anbar, A. D. and Lyons, T. W. (2009) A late Archean sulfidic sea stimulated by early oxidative weathering of the continents. *Science, 326*, 713-716. doi: 10.1126/science.1176711

Romaniello, S. J., Herrmann, A. D. and Anbar, A. D. (2013) Uranium concentrations and 238U/235U isotope ratios in modern carbonates from the Bahamas: Assessing a novel paleoredox proxy. *Chemical Geology, 362*, 305-316. doi: 10.1016/j.chemgeo.2013.10.002

Saltzman, M. R., and Young, S. A. (2005) Long-lived glaciation in the Late Ordovician? Isotopic and sequence-stratigraphic evidence from western Laurentia. *Geology, 33*(2), 109. doi: 10.1130/g21219.1

Schauble, E. A. (2007) Role of nuclear volume in driving equilibrium stable isotope fractionation of mercury, thallium, and other very heavy elements. *Geochimica et Cosmochimica Acta, 71*(9), 2170-2189. doi: 10.1016/j.gca.2007.02.004

Scott, C. and Lyons, T. W. (2012) Contrasting molybdenum cycling and isotopic properties in euxinic versus non-euxinic sediments and sedimentary rocks: Refining the paleoproxies. *Chemical Geology, 324-325*, 19-27. doi: 10.1016/j.chemgeo.2012.05.012

Scott, C., Lyons, T. W., Bekker, A., Shen, Y., Poulton, S. W., Chu, X. and Anbar, A. D. (2008) Tracing the stepwise oxygenation of the Proterozoic ocean. *Nature, 452*(7186), 456-459. doi: 10.1038/nature06811

Selby, D., Creaser, R. A. and Fowler, M. G. (2007) Re–Os elemental and isotopic systematics in crude oils. *Geochimica et Cosmochimica Acta, 71*(2), 378-386. doi: 10.1016/j.gca.2006.09.005

Siebert, C., McManus, J., Bice, A., Poulson, R. L. and Berelson, W. M. (2006) Molybdenum isotope signatures in continental margin marine sediments. *Earth and Planetary Science Letters, 241*(3-4), 723-733. doi: 10.1016/j.epsl.2005.11.010

Siebert, C., Nägler, T. F., von Blanckenburg, F. and Kramers, J. D. (2003) Molybdenum isotope records as a potential new proxy for paleoceanography. *Earth and Planetary Science Letters, 211*(1-2), 159-171. doi: 10.1016/s0012-821x(03)00189-4

Sheehan, P. M. (2001) The late Ordovician mass extinction. *Annual Review of Earth and Planetary Sciences, 29*, 331-364.

Shields, G. A., Carden, G. A. F., Veizer, J., Meidla, T., Rong, J. and Li, R. (2003) Sr, C, and O isotope geochemistry of Ordovician brachiopods: a major isotopic event around the Middle-Late Ordovician transition. *Geochimica et Cosmochimica Acta, 67*(11), 2005-2025. doi: 10.1016/s0016-7037(02)01116-x

Stein, H. J., Hannah, J. L., Yang, G., Galimberti, R. and Nali, M. (2014) Ordovician Source Rocks and Devonian Oil Expulsion on Bolide Impact at Siljan, Sweden - The Re-Os Story. *Society of Petroleum Engineers - International Petroleum Technology Conference 2014, IPTC 2014 Unlocking Energy Through Innovation, Technology and Capability, 4*, 3212-3217.

Stein, H. J., Hannah, J. L., Zimmerman, A. and Egenhoff, S. (2009) Re-Os fractionation on instantaneous maturation at the Siljan meteorite impact site, central Sweden. *Geochimica et Cosmochimica Acta*, A1268.

Stirling, C. H., Andersen, M. B., Potter, E. and Halliday, A. N. (2007) Low-temperature isotopic fractionation of uranium. *Earth and Planetary Science Letters, 264*(1-2), 208-225. doi: 10.1016/j.epsl.2007.09.019

Svensson, N. B. (1973) Shatter cones from the Siljan struture, central Sweden. *Geologiska Föreningen i Stockholm Förhandlingar, 95*, 139-143.

Tamminen, J. and Wickman, F. E. (1980) Shock effects in pegmatitic quartz from the Siljan ring structure, central Sweden. *Geologiska Föreningen i Stockholm Förhandlingar, 102*, 275-278.

Telus, M., Dauphas, N., Moynier, F., Tissot, François L. H., Teng, F., Nabelek, P. I., Craddock, P. R. and Groat, L. A. (2012) Iron, zinc, magnesium and uranium isotopic fractionation during continental crust differentiation: The tale from migmatites, granitoids, and pegmatites. *Geochimica et Cosmochimica Acta, 97*, 247-265. doi: 10.1016/j.gca.2012.08.024

Tissot, F. L. H. and Dauphas, N. (2015) Uranium isotopic compositions of the crust and ocean: Age corrections, U budget and global extent of modern anoxia. *Geochimica et Cosmochimica Acta, 167*, 113-143. doi: 10.1016/j.gca.2015.06.034

Tribovillard, N., Algeo, T. J., Lyons, T. W. and Riboulleau, A. (2006) Trace metals as paleoredox and paleoproductivity proxies: An update. *Chemical Geology, 232*(1-2), 12-32. doi: 10.1016/j.chemgeo.2006.02.012

Trotter, J. A., Williams, I. S., Barnes, C. R., Lécuyer, C. and Nicoll, R. S. (2008) Did Cooling Oceans Trigger Ordovician Biodiversification? Evidence from Conodont Thermometry. *Science, 321*, 550-554.

Vlierboom, F. W., Collini, B. and Zumberge, J. E. (1986) The occurrence of petroleum in sedimentary rocks of the meteor impact crater at Lake Siljan, Sweden. *Organic Geochemistry, 10*, 153-161.

Webby, B. D., Paris, F., Droser, M. L. and Percival, I. G. (2004) The Great Ordovician Biodiversification Event: Columbia University Press, New York. 484 pp.

Weyer, S., Anbar, A. D., Gerdes, A., Gordon, G. W., Algeo, T. J. and Boyle, E. A. (2008) Natural fractionation of 238U/235U. *Geochimica et Cosmochimica Acta, 72*(2), 345-359. doi: 10.1016/j.gca.2007.11.012

Yan, D., Chen, D., Wang, Q., Wang, J. and Wang, Z. (2009) Carbon and sulfur isotopic anomalies across the Ordovician–Silurian boundary on the Yangtze Platform, South China. *Palaeogeography, Palaeoclimatology, Palaeoecology, 274*(1-2), 32-39. doi: 10.1016/j.palaeo.2008.12.016

Zhang, T., Shen, Y., Zhan, R., Shen, S. and Chen, X. (2009) Large perturbations of the carbon and sulfur cycle associated with the Late Ordovician mass extinction in South China. *Geology, 37*(4), 299-302. doi: 10.1130/g25477a.1

Zhang, T., Trela, W., Jiang, S. Y., Nielsen, J. K. and Shen, Y. (2011) Major oceanic redox condition change correlated with the rebound of marine animal diversity during the Late Ordovician. *Geology, 39*(7), 675-678. doi: 10.1130/g32020.1

Zhou, L., Algeo, T. J., Shen, J., Hu, Z., Gong, H., Xie, S., Huang, J. and Gao, S. (2015) Changes in marine productivity and redox conditions during the Late Ordovician

Hirnantian glaciation. *Palaeogeography, Palaeoclimatology, Palaeoecology, 420*, 223-234. doi: 10.1016/j.palaeo.2014.12.012

Zhou, L., Wignall, P. B., Su, J., Feng, Q., Xie, S., Zhao, L. and Huang, J. (2012) U/Mo ratios and δ98/95Mo as local and global redox proxies during mass extinction events. *Chemical Geology, 324-325*, 99-107. doi: 10.1016/j.chemgeo.2012.03.020